Relationship Between Neuroendocrine and Immune Gene Expression in Small Cell Lung Cancer

Ling Cai (ling.cai@utsouthwestern.edu)
The University of Texas Southwestern Medical Center
Hongyu Liu
The University of Texas Southwestern Medical Center
fang huang
The University of Texas Southwestern Medical Center
Junya Fujimoto
MD Anderson Cancer Center
Luc Girard
The University of Texas Southwestern Medical Center
Jun Chen
Tianjin Medical University General Hospital
Yongwen Li
Tianjin Medical University General Hospital
Yu-an Zhang
The University of Texas Southwestern Medical Center
Dhruba Deb
The University of Texas Southwestern Medical Center
Victor Stastny
The University of Texas Southwestern Medical Center
Christin Kuo
Stanford University
Gaoxiang Jia
The University of Texas Southwestern Medical Center
Chendong Yang
The University of Texas Southwestern Medical Center
Wei Zou
Roche (United States)
Adeeb Alomar
The University of Texas Southwestern Medical Center
Kenneth Huffman
University of Texas Southwestern Medical Center
Mahboubeh Papari-Zareei

The University of Texas Southwestern Medical Center
Lin Yang
Chinese Academy of Medical Sciences & Peking Union Medical College
Benjamin Drapkin
The University of Texas Southwestern Medical Center
Esra Akbay
UT Southwestern
David Shames
Roche (United States)
Ignacio Wistuba
M. D. Anderson Cancer Center
Tao Wang
The University of Texas Southwestern Medical Center https://orcid.org/0000-0002-4355-149X
Guanghua Xiao
UT Southwestern Medical Center
Ralph DeBerardinis
The University of Texas Southwestern Medical Center https://orcid.org/0000-0002-2705-7432
John D. Minna
University of Texas Southwestern Medical Center https://orcid.org/0000-0002-7776-0767
Yang Xie
The University of Texas Southwestern Medical Center
Adi Gazdar
The University of Texas Southwestern Medical Center

Article

Keywords: small cell lung cancer, neuroendocrine, immune gene expression, lung cancer

Posted Date: August 4th, 2020

DOI: https://doi.org/10.21203/rs.3.rs-50416/v1

Version of Record: A version of this preprint was published at Communications Biology on March 9th, 2021. See the published version at https://doi.org/10.1038/s42003-021-01842-7.

Relationship Between Neuroendocrine and Immune Gene Expression in Small Cell Lung Cancer

Ling Cai[1,2,3,*], Hongyu Liu[1,4], Fang Huang[2], Junya Fujimoto[5], Luc Girard[3,6,7], Jun Chen[4,8], Yongwen Li[4], Yu-an Zhang[6], Dhruba Deb[6], Victor Stastny[6], Christin S. Kuo[9], Gaoxiang Jia[1], Chendong Yang[2], Wei Zou[10], Adeeb Alomar[6], Kenneth Huffman[6], Mahboubeh Papari-Zareei[6], Lin Yang[11], Benjamin Drapkin[3,6,12], Esra Akbay[13], David S. Shames[10], Ignacio I. Wistuba[5], Tao Wang[1,3], Guanghua Xiao[1,3,14], Ralph J. DeBerardinis[2,3,15], John D. Minna[3,6,7,12,*], Yang Xie[1,3,14,*], Adi F. Gazdar[3,6,13,v]

Affiliations

[1]Quantitative Biomedical Research Center, Department of Population and Data Sciences, UT Southwestern Medical Center, Dallas, TX 75390, USA.

[2]Children's Research Institute, UT Southwestern Medical Center, Dallas, TX 75390, USA.

[3]Simmons Comprehensive Cancer Center, UT Southwestern Medical Center, Dallas, TX 75390, USA.

[4]Tianjin Key Laboratory of Lung Cancer Metastasis and Tumor Microenvironment, Tianjin Lung Cancer Institute, Tianjin Medical University General Hospital, Tianjin 300052, People's Republic of China.

[5]Department of Translational Molecular Pathology, University of Texas MD Anderson Cancer Center, Houston, TX 77054, USA.

[6]Hamon Center for Therapeutic Oncology Research, University of Texas Southwestern Medical Center, Dallas, TX 75390, USA.

[7]Department of Pharmacology, UT Southwestern Medical Center, Dallas, TX 75390, USA.

[8]Department of Lung Cancer Surgery, Tianjin Lung Cancer Institute, Tianjin Medical University General Hospital, Tianjin 300052, People's Republic of China.

[9]Department of Pediatrics, Stanford University, CA 94305, USA

[10]Department of Oncology Biomarker Development, Genentech Inc., South San Francisco, CA 94080, USA

[11]Department of Pathology, National Center/Cancer Hospital, Chinese Academy of Medical Sciences and Peking Union Medical College, Beijing, China

[12]Department of Internal Medicine, University of Texas Southwestern Medical Center, Dallas, TX 75390, USA.

[13]Department of Pathology, UT Southwestern Medical Center, Dallas, TX 75390, USA.

[14]Department of Bioinformatics, University of Texas Southwestern Medical Center, Dallas, TX 75390, USA.

[15]Howard Hughes Medical Institute, University of Texas Southwestern Medical Center, Dallas, TX 75390, USA.

[▿] Deceased

[*]Correspondence to Ling.Cai@UTSouthwestern.edu, John.Minna@UTSouthwestern.edu and Yang.Xie@UTSouthwestern.edu

ABSTRACT

Small cell lung cancer (SCLC) is classified as a high-grade neuroendocrine (NE) tumor, but a subset of SCLC has been termed “variant” due to the loss of NE characteristics. In this study, we computed NE scores for patient-derived SCLC cell lines and xenografts, as well as human tumors. We aligned NE properties with transcription factor-defined molecular subtypes. Then we investigated the different immune phenotypes associated with high and low NE scores. We found repression of immune response genes as a shared feature between classic SCLC and pulmonary neuroendocrine cells of the healthy lung. With loss of NE fate, variant SCLC tumors regain cell-autonomous immune gene expression and exhibit higher tumor-immune interactions. Pan-cancer analysis revealed this NE lineage-specific immune phenotype in other cancers. Additionally, we observed MHC I re-expression in SCLC upon development of chemoresistance. These findings provide a new framework to guide design of treatment regimens in SCLC.

INTRODUCTION

Small cell lung cancer (SCLC), accounting for 15% of lung cancer cases, with a 5-year survival of 6%, is designated by the US Congress as a “recalcitrant cancer” (1, 2). SCLC is classified as a high-grade neuroendocrine (NE) tumor (3). A large fraction of SCLC tumors are driven by *ASCL1,* a lineage oncogene also important for pulmonary neuroendocrine cell (PNEC) fate determination (4, 5). In healthy lung tissue, PNECs are rare and dormant (6), whereas upon lung injury, some act as stem cells to regenerate surrounding epithelial cells (7). SCLC occurs primarily in heavy smokers, but despite the very high mutation burden (8-10) from SCLC genomes predicted to contribute an ample supply of neoantigens, SCLCs express low levels of major histocompatibility complex class I (MHC I) proteins to present tumor-specific antigens (11, 12). This could explain why, among various types of cancer, checkpoint-blockade immunotherapy (CBI) underperforms in SCLC (13, 14).

Thirty-five years ago, it was observed that by contrast to “classic” SCLC cell lines (which grew in tissue culture as floating cell aggregates), a subset of patient-derived SCLC lines behaved differently - growing as adherent monolayers in culture, with morphologically larger cells, more prominent nucleoli, and expressed few or no NE markers (15, 16). These characteristics led such tumors to be termed “variant” or “non-NE”

SCLC. Many of these variant SCLC lines were established from patients whose tumors had acquired resistance to chemotherapy and clinically relapsed, a context in which genomic *MYC* amplification was also noted to be more frequent (17). Notch activation had been shown to mediate the transition from "classic" to "variant" subtypes and accounts for the intratumoral heterogeneity commonly seen in SCLC (18).

Recently, extending the concepts of "classic" and "variant" SCLC, both intertumoral, and intratumoral heterogeneity in SCLC has been documented and has been associated with expression of lineage-specific transcription factors (TFs) *ASCL1*, *NEUROD1*, *YAP1*, and *POU2F3*, and these various subtypes express different levels of NE markers (19-21).

We have previously defined a 50-gene NE signature that helps us quantify the NE properties as a continuous NE score ranging from -1 to 1, with a more positive score indicating higher NE properties (22). In the current study we applied this NE scoring method to SCLC samples from preclinical models and patient tumors. We first assessed the relationship between NE scores and SCLC molecular subtypes. Then, we investigated the immune phenotypes associated with variable NE scores in SCLC and other cancer types.

RESULTS

Relationship between NE scores and SCLC molecular subtypes

Using the 50-gene NE signature updated with all available SCLC-related RNA-seq data (**Table S1**), we computed NE scores for patient-derived SCLC lines and xenografts (PDXs) as well as four independent patient tumor datasets (including one newly generated for this study) (**Tables 1** and **S2**). We examined the relationship between NE scores and expression of SCLC molecular subtype-specific TFs as proposed by Rudin et al (**Figure 1a-b**). Our findings are largely consistent with the previous proposal that assigns ASCL1+ and NEUROD1+ SCLCs to NE subtypes and POU2F3+ and YAP1+ SCLCs to non-NE subtypes. However, we note some discrepancies. First, we found that while expression of *ASCL1* and *NEUROD1* seems to be mutually exclusive in cell lines, they seem to co-express in many of the tumor samples; secondly, in "George_2015", "Jiang_2016" and our own dataset, we have observed rare POU2F3+ samples that have high NE scores.

With serially sectioned formalin fixed paraffin embedded (FFPE) slides from 9 out of the 18 tumors for which we had performed expression profiling, we examined the tumors with hematoxylin and eosin (H&E) staining as well as immunohistochemistry (IHC) staining of ASCL1, NEUROD1 and POU2F3 (**Figures 1c-f**). The high NE-score tumors exhibited predominantly classic SCLC morphology with dark nuclei, scant cytoplasm and inconspicuous nucleoli. Notably, this was not only seen in ASCL1+ tumors (for example, SCLC-04, NE score 0.4) but also in the POU2F3+ tumor with a positive NE-score (SCLC-15, NE score 0.26) (**Figure 1c**). On the other hand, while we observed variant morphology in tumors with low NE scores, we noticed intratumoral heterogeneity. In a tumor weakly positive for ASCL1 (SCLC-20, NE score -0.05), the ASCL1-high regions were found to be more "classic"-like whereas the ASCL1-low regions were more "variant"-like (**Figure 1d**). Our IHC-based quantifications largely agree with the microarray gene expression assessments (**Figure 1e**). Tumors that were found to express both *ASCL1* and *NEUROD1* stained positive for both markers as well. In addition, intratumoral heterogeneity was commonly found within such tumors, where there are areas with high expression of both TFs but also areas with expression of only one TF (**Figure 1f**).

Immune gene repression is a NE lineage-specific property

We performed correlation between NE scores and SCLC transcriptomic data to identify gene expression changes associated with the NE program. Not surprisingly, gene ontology (GO) analyses revealed genes related to the neuronal system as highly expressed in high NE-score samples (**Figures S1a-b**). By contrast, genes negatively associated with NE score were enriched for GO terms related to immune response, and this was observed in both the cell line and human tumor datasets (**Figure S1c-d**). We also performed gene set enrichment analysis (GSEA) (23) with a variety of gene set libraries collected by Enrichr (24). Consistent with previous report that Notch signaling dependent REST (Neuron-Restrictive Silencer Factor) activation represses neuronal gene expression in variant SCLC (18), we found REST targets (i.e. repressed by REST) are abundantly expressed in high NE-score SCLCs. On the other hand, interferon-stimulated genes (ISGs) are found to highly express in the low NE-score (variant) SCLC samples (**Figures 2a-b**). As NFκB signaling mediates activation of ISGs, we examined reverse phase protein array (RPPA) data from the cancer cell

line encyclopedia (CCLE) (25) and found higher levels of activating serine 536 phosphorylation on p65 (26) in low NE-score SCLC lines (**Figure 2c**).

Our 50-gene signature derived from lung cancer cell line mRNA data (**Table S1**) contains several genes with immune related functions that were found to highly express in variant SCLC. Some are involved in cytokine signaling; for example, *IL18* encodes for a proinflammatory cytokine (27), and *OSMR* encodes for a receptor for oncostatin M and IL-31 (28). Furthermore, many of these genes are involved with immunosuppressive processes, including *NT5E* (29), *TGFBR2* (30), *ANXA1 (31)*, *EPHA2 (32)*, *HFE* (33) and *LGALS3* (34). Our pathway analyses indicates that beyond these genes included in the NE expression signature, there is a broad immune program concertedly upregulated in low NE-score SCLC samples. We extended our analysis to a few immune gene sets that were previously identified to express cell autonomously in cancer. These gene sets include the following: SPARCS genes (stimulated 3 prime antisense retroviral coding sequences) reported to express in mesenchymal tumors and mediate interferon-gamma signal amplification (35); "parainflammation" (PI) genes in epithelial tumor cells (36); and senescence-associated secretory phenotype (SASP) genes (37) that reinforce the senescence arrest, alter the microenvironment, and trigger immune surveillance of the senescent cells (38). We observed that the expression these genes also negatively correlate with NE scores in SCLC despite little overlap among genes in these various sets (**Figure S2**).

While the expression of neuronal program genes in in high NE-score SCLCs can be attributed to the NE lineage, we examined single-cell RNA-seq (scRNA-seq) data from the healthy human lung epithelial cells (39) to check whether the expression repression of ISGs is also a lineage-specific phenomenon that could be observed in PNECs rather than being cancer-specific. Consistent with the previous report that ASCL1 negatively regulate YAP1 during neuronal differentiation (40), the highest expression of *ASCL1* and lowest expression of *YAP1* were observed in PNECs, relative to other cell types. We confirmed that while PNECs have increased expression of REST target genes, ISGs are indeed repressed as well (**Figure 2d and S3a**). Additionally, we specifically examined interferon receptors in PNECs and found that they also have the lowest expression in PNECs (**Figures 2d**), suggesting that besides repression of basal ISG expression, in

the presence of interferon stimulation, PNECs would also be less primed for further activation of ISGs. It has been estimated that 10% of the genes in the human genome have the potential to be regulated by IFN, many ISGs work in immune defense against viral infection, but some could be hijacked by viruses (41). As some PNECs are rare stem cells, we reason that ISG repression could lower their risk from viral infection. In the context of the current COVID-19 pandemic, we examined scRNA-seq data from Ouadah et al., who performed lineage tracing with an *Ascl1*^{CreERT2}*; Rosa26*$^{LSL\text{-}ZsGreen}$ mouse model to show that some PNECs can transdifferentiate into other cell types (7). **Figure S3b** generated with their data shows that AT2 and ciliated cells originated from PNECs in this model have lost *Ascl1* but increased *Yap1* expression. *Ly6e* and *Tmprss2*, genes involved in coronavirus defense (42) and hijacked entry (43) respectively, were also upregulated.

Increased tumor-immune interaction in low NE-score SCLC tumor samples

It has been long observed that expression of MHC I is low in SCLC (11). Using single sample gene set enrichment analysis (ssGSEA) (44), we derived the MHC I scores for MHC I genes. From studies that had collected lung tumors of different histology, MHC I scores positively correlate with *PTPRC* (which encodes for pan-leukocyte marker CD45) levels (**Figures 3a and S4a**). The lowest MHC I and *PTPRC* gene expression were found in neuroendocrine tumors, including not only SCLC but also carcinoids (**Figure 3a**), suggesting these NE tumors with decreased MHC I have fewer immune infiltrates. In SCLC datasets, low NE-score samples exhibited upregulation of MHC I genes (**Figure 3b**) and were associated with higher *PTPRC* expression in patient tumor datasets (**Figure S4b**). We also estimated immune cell infiltration by deriving immune cell type-specific signature scores (45) and found that they negatively correlate with NE scores in SCLC patient tumors, suggesting increased tumor-immune interaction in low NE-score tumors (**Figure 3c**).

We saw higher expression of PD-L1 (CD274) in low NE-score SCLCs (**Figure S5a**). Furthermore, genes from an IFN-gamma related signature that has been shown to predict PD-1 blockade response in multiple cancer types (46) are highly expressed in low NE-score SCLC tumors across multiple datasets (**Figure 3c**). We also examined a list of 21 immune checkpoint genes (47), immune suppressive cytokines (IL-10 and

TGF-beta), and their receptors (48), for their association with NE scores. We found that these genes also have higher expression in low NE-score SCLC tumors (**Figure 3c**). Finally, the expression of 995 immunosuppressive genes from the Human Immunosuppression Gene Atlas (47) were assessed and again, the majority of these genes exhibit negative correlation between mRNA expression and NE scores across different SCLC tumor datasets (**Figure S5b** and **Table S3**).

Besides gene expression-based analyses, we also performed immunohistochemistry (IHC) with our 9 SCLC tumor samples to quantify tumor infiltrating CD8+ and CD4+ T cells (**Table S2**). Of importance, both intratumoral and intertumoral heterogeneity were observed in T cell infiltration. Within the same tumor, areas with low tumor ASCL1 levels exhibited more CD8+ and CD4+ T cell infiltration, whereas areas with high tumor ASCL1 levels showed fewer CD8+ or CD4+ T cells (**Figure 4a**). Across all the SCLC tumor specimens assessed, CD8+ and CD4+ T cell per area cell count positively correlated with the T cell score computed from gene expression data, and both IHC-based T cell counts and gene expression-based T cell scores negatively correlated with NE scores (**Figure 4b**).

Pan-cancer analyses for NE score expression and immune response genes.

These findings had prompted us to examine other cancer types to see whether immune gene repression is seen in other NE tumors and whether “variant” subtype from NE lineage loss could also be observed (**Figure 4c**). A recent study identified “SCLC-like” epithelial tumors in pan-cancer samples using a principal component analysis-based approach. They found that tumors across many lineages with a higher “SCLC-like” score had lower immune gene expression (49). We applied our NE scoring method across all cancer lineages (“pan-cancer” analysis) to compute NE scores and assess their relationship with immune phenotypes. In pediatric (Therapeutically Applicable Research to Generate Effective Treatments – TARGET) and adult (The Cancer Genome Atlas – TCGA) pan-cancer studies (50), neuroendocrine tumor neuroblastoma (NBL), as well as pheochromocytoma & paraganglioma (PCPG) were identified as containing the highest NE scores (**Figures 5a-b**). Tumors of glial origin, including Low Grade Glioma (LGG) and Glioblastoma Multiforme (GBM) also have high NE scores. Besides these NE/glial tumors, a small number of high NE-score samples were observed for bladder urothelial carcinoma (BLCA), breast invasive

carcinoma (BRCA), lung adenocarcinoma (LUAD), lung squamous cell carcinoma (LUSC), pancreatic adenocarcinoma (PDAC) and stomach adenocarcinoma (STAD), for which it is also known that neuroendocrine tumors, while uncommon, still comprise a small proportion of the cases (**Figures 5a-b**). Previous immunogenomic analysis had classified pan-cancer TCGA samples into six immune subtypes (51). We found samples from the "immunologically quiet" subclass have the highest NE score, followed by the "lymphocyte depleted" subclass (**Figure 5c**). We further assessed the relationship between NE scores and the tumor-infiltrating lymphocytes and leukocyte regional fractions previously reported for the pan-cancer samples (51), these immune metrics negatively correlate with NE scores across all samples (**Figure 5d**) and also within specific tumor types (**Figure S6**).

We took a close examination of NBL using cell line expression data from CCLE (25) along with patient tumor data from TARGET (52) for lineage factors *ASCL1* and *YAP1*, REST targets, ISGs, MHC I, immune cell-specific signature scores (45), Ayer et al.'s PD-1 blockade response signature (46), immune checkpoints (47) and suppressive cytokines and receptors (48). The pattern for NBL (**Figure 5e**) highly resembles that of SCLC (**Figures 2a, 3b-c**) suggesting the existence of a "variant" NBL subset with decreased neuroendocrine features, increased cell-autonomous expression of immune genes as well as increased tumor-immune interaction. Like SCLC, we also found higher levels of NFkB-p65 phosphorylation in the low NE-score variant NBL cell lines (**Figure 5f**).

MHC I re-expression in chemoresistant SCLC

As it was previously observed that variant SCLC cell lines were frequently derived from patients whose tumors had relapsed on chemotherapy (17), we wondered if the development of chemo-resistance in tumors was associated with the altered expression of immune genes, especially MHC I. Five sets of data with origin-matched chemosensitive and chemoresistant samples were examined to address this question. In 2017, using a genetically engineered mouse model (GEMM), Lim et al showed that Notch-active SCLC cells were more chemoresistant (18). Using their data we found the Notch active SCLC cells had switched from ASCL1+ to YAP1+, have reduced NE scores and increased expression of ISGs and MHC I genes (**Figure 6a**). We next examined a series of preclinical models we and others have developed for human

SCLC. Classic, high NE-score SCLC cell lines predominantly grow as floating aggregates in culture, but contain a small proportion of cells growing adherently in a monolayer. By selecting for adherent growth, we generated an adherent subline H69-AD(/NCI-H69-AD) from parental, chemosensitive H69(/NCI-H69) cells (**Figure 6b**). Increased resistance to Cisplatin (~10 fold) and Etoposide (~6 fold) was observed in H69-AD compared to the parental H69 cells (**Figure 6c**). We found H69-AD had transitioned to become a low NE-score (-0.02) YAP1+ variant line compared to the parental high NE-score (0.91) classic ASCL1+ line. Both ISGs and MHC I genes were found to have increased expression in H69-AD (**Figure 6d**). In a previous study, Cañadas et al. also derived sublines from H69. Hepatocyte growth factor treatment was used to induce mesenchymal transition of H69 cells, resulting in H69-M lines that were found to be chemoresistant both *in vitro* and *in vivo* (53). From their dataset, we also found MHC I expression increased in H69-M compared to parental H69 cells. There was some increase in ISGs too, but less prominent compared to H69-AD from us. Notably, although *YAP1* expression increased in H69-M, *ASCL1* levels did not change (**Figure 6d**). As the fourth set of data, PDX models established sequentially from SCLC tumors ("Drapkin_2018") collected before and after chemotherapy from the same patient (54) were examined. In PDXs from patient MGH1518 for which chemoresistance had developed in the relapsed sample, we found upregulation of MHC I, but not ISGs (**Figure 6d**). Of note, this relapsed sample maintained a high NE score, but expressed higher levels of *MYC*, consistent with previous findings that MYC mediates chemoresistance (54). Lastly, we generated a set of subcutaneous xenograft models from a high NE-score human SCLC cell line NCI-H1436 with or without selection for resistance to Cisplatin and Etoposide in the mice (**Figure 6e**). Compared to the parental xenograft, the drug resistant xenografts maintained *ASCL1* expression but exhibited increased *B2M* (MHC I complex subunit), *PSMB8* (immunoproteasome subunit) (**Figure 6e**), and *MYC* (Fang Huang's manuscript under review at JCI). Collectively, these findings suggest MHC I can re-express upon development of chemoresistance - in some cases, with lineage transition; and in some other cases, accompanied by an increase in *MYC* expression.

We also checked whether expression levels of MHC I and *MYC* differ by tumor source and anatomical site based on the "NCI/Hamon Center" patient-derived SCLC lines dataset (**Figures S7**). Interestingly, the lowest MHC I and *MYC* levels were both observed for cell lines derived from primary site lung tumor

specimens and they are all high-NE tumors, whereas higher MHC I levels were observed in SCLC lines isolated from metastatic tumor samples especially those from lymph node and bone marrow. These observations remain to be validated with primary and metastatic samples from the same patients.

DISCUSSION

In this study, we examined NE properties of patient-derived SCLC cell lines, PDXs and human tumors based on NE scores estimated from a gene expression signature. Currently, it is believed that Notch activation drives the lineage transition from ASCL1+ to NEUROD1+ to YAP1+ subtype (55) whereas POU2F3+ SCLC is a standalone subtype originated from tuft cells (56). While we observed mutually exclusive patterns of *ASCL1* and *NEUROD1* expression in cell lines, their co-expression was identified in many patient tumors. Our IHC results further revealed intratumoral heterogeneity in such tumors, suggesting ongoing lineage transition in primary treatment naïve tumors. From alignment of NE scores and molecular subtype-specific TF expression, we observed rare high NE-score POU2F3+ tumors in three independent datasets, raising the possibility that POU2F3+ tumors could also arise from NE lineage.

Our investigation of immune phenotypes associated with variable NE scores had identified repression of ISGs in classic high NE-score SCLC. While it remains to be determined what other pulmonary cells besides PNECs can function as “cells of origin” for SCLC (57-60), the gene expression similarities between PNECs and SCLC suggests many of the SCLC properties could be tied to PNEC characteristics. We confirmed ISG repression in PNECs relative to other lung epithelial cells through examination of scRNA-seq data from healthy human lung. ISGs provide viral defense for cells but some can be hijacked by viruses (41). Since PNECs assume stem cell roles for tissue regeneration after injury (7), lowering expression of ISGs and other genes involved in viral entry presumably play some role in self-protection. Like SCLC, PNECs can switch from ASCL1+ to YAP1+ through Notch activation, but in the context of tissue repair (7). Our findings suggest that the increase of cell autonomous immune gene expression as high NE-score SCLCs transition to low NE-score SCLCs is mirroring the changes that normally take place during the transdifferentiation of PNECs to other lung epithelial cell types, and in SCLC, this had in turn led to an increased tumor-immune interaction. Interestingly, our pan-cancer analysis had extended this finding of reciprocal relationship

between neuroendocrine and immune gene expression to other cancer types. For NBL, a cancer that had not previously been classified based on NE properties, we were able to identify more inflammatory variant tumors with loss of NE lineage gene expression. It would be interesting to explore more of such molecular similarities between SCLC and other tumors with NE/neuronal lineage.

The full repertoire of immune evasion strategies employed by SCLC remains to be elucidated. However, our results tying together with current clinical treatment findings raise several important questions and paradoxes. The first paradox is that we found a depletion of immune infiltrates in high NE-score SCLC tumors and other neuroendocrine tumors (NETs), associated with down regulation of MHC I expression. While this MHC I expression explains the presence of very few T cells, it raises the question of how high NE-score NETs evade natural killer cells that normally would recognize the "missing self" that such MHC I expression loss conveys (61). Thus, we feel the high NE-score low-MHC I expression pairing indicates we need to understand how natural killer cell mechanisms are avoided in NET pathogenesis. The second paradox is that low NE-score "variant" SCLCs appear to be associated with expression of MHC I and a more immune infiltrated tumor microenvironment, yet clinical trials of immune checkpoint blockade do not clearly show these are the tumors responding to such therapy. Since we found these tumors also express many immunosuppressive genes it will be important to know which of these immunosuppressive gene functions need to be targeted to achieve anti-tumor immune responses. Finally, we observed expression of MHC I in selected SCLC samples with chemoresistance and increased *MYC* expression even without changes in ASCL1 expression. We need to know if immunosuppressive mechanisms are the same or different in the high vs. low NE-score SCLC resistant to chemotherapy. We conclude, that some 30 years after the first description of "classic" (high NE-score) and "variant" (low NE-score) SCLCs there are important links between these NE phenotypes and the expression of immune phenotypes, and between similar gene expression profiles of SCLC and pulmonary neuroendocrine cells. Importantly, these correlations identify important problems to be solved of clinical therapeutic translational relevance.

Source	Name	Tissue Source	Sample Type	n	Reference
Human	SCLC cell lines/ NCI/Hamon Center	SCLC	Cell line	69	This study
Human	Cañadas_2014	SCLC	Cell line	6	(53)
Human	Drapkin_2018	SCLC	PDX	19	(54)
Human	Rudin_2012	SCLC	Tumor	29	(9)
Human	George_2015	SCLC	Tumor	81	(10)
Human	Jiang_2016	SCLC	Tumor	79	(62)
Human	SCLC tumors (this study)	SCLC	Tumor	18	This study
Human	expO	Lung cancer	Tumor	109	(63)
Human	Rousseaux_2013	Lung cancer	Tumor	286	(63, 64)
Human	CCLE	Pan-cancer	Cell line	-	(25)
Human	TCGA	Pan-cancer	Tumor	10535	(50)
Human	TARGET	Pan-cancer	Tumor	734	(50)
Mouse	Lim_2017	SCLC	Pooled FACS sorted tumor cells ^	6	(18)
Human	Travaglini_2020	Healthy lung	Single cell	9384*	(39)
Mouse	Ouadah_2019	Healthy lung	Single cell	46*	(7)

Table 1. Datasets used for analyses

PDX, Patient-deived Xenografts; FACS, Fluorescence-activated cell sorting; scRNA-seq, Single-cell RNA sequencing; * cells; - Note that CCLE datasets were used in multiple analyses with different numbers of cell lines; ^ In Lim_2017, *Rb1*$^{flox/flox}$;*p53*$^{flox/flox}$;*p130*$^{flox/flox}$;*R26*^{mTmG}; *Hes1*$^{GFP/+}$ GEMM SCLC tumors were initiated by Ad-CMV-Cre, sorted by Tomato and GFP to obtain relatively pure tumor cells.

FIGURE LEGENDS

Figure 1 NE score and SCLC molecular subtypes

a, Heatmaps visualizing expression of molecular subtype-specific TFs and NE scores. Two heatmaps were generated for each study, with one ordered by complete linkage hierarchical clustering of TFs and the other ordered by NE scores. **b**, Pairwise associations among NE scores and molecular subtype-specific TFs. Lower left panels are scatter plots, diagonal line panels are density plots and upper right panel shows correlation coefficients from pairwise Pearson correlation. *, p-value < 0.05. **c**, H&E staining of two high NE-score SCLC tumor samples showing classic SCLC morphology with dark nuclei, scant cytoplasm and inconspicuous nucleoli. **d**, ASCL1 IHC staining and H&E staining of a low NE-score SCLC tumor, showing variable morphology at different selected areas, where ASCL1-low areas appear to be more variant-like **e**, Quantifications of TF expression from IHC staining or microarray profiling, samples are ordered by increasing NE scores. **f**, IHC of ASCL1, NEUROD1 and POU2F3 in two tumors that express both ASCL1 and NEUROD1. Two areas per tumor were selected for showing intratumoral heterogeneity in ASCL1 and NEUROD1 expression patterns.

Figure 2 Repression of ISGs in high NE-score SCLC and PNECs

a, GSEA enrichment plots for selected genesets. Results from SCLC cell lines, PDXs (Drapkin_2018) and patient tumor datasets were superimposed. Normalized enrichment score (NES) were provided. *, multiple comparison adjusted p-value < 0.05. **b**, Heatmaps for top 25 leading edge genes selected from genesets in (**a**). Gene expression matrix of each dataset was annotated with color-coded Pearson correlation coefficient (from correlating NE score with gene expression) as a left-side column, and a top bar indicating NE scores. **c**, Scatter plots showing negative correlation between NE score and Ser536 phosphorylation on NFkB-p65 in SCLC cell lines. Pearson correlation coefficient was provided. *, p-value < 0.05. **d**, Heatmap showing relative expression of selected lineage factors (*ASCL1* and *YAP1*), REST targets and ISGs (same genes as used in **b,** determined from **a**) as well as interferon receptor genes in healthy human lung epithelial cells based on scRNA-seq experiments.

Figure 3 Low NE-score variant SCLC have increased tumor-immune interaction

a, Expression of MHC I genes and pan-leukocyte marker *PTPRC* in lung tumors from the "Rousseaux_2013" dataset. Box whisker plots are filled with color reflecting the median NE score in different histological subtypes. Color for scatterplot symbols reflects NE score for different samples. **b**, Heatmaps visualizing expression of MHC I genes across multiple SCLC datasets. **c**, Heatmaps visualizing expression of *PTPRC*, immune-cell-type-specific signature scores, PD-1 blockade response-predicting IFN-gamma related signature genes (46), immune checkpoint genes and suppressive cytokines and receptors in SCLC tumor datasets.

Figure 4 Intertumoral and intratumoral heterogeneity in T cell infiltration from SCLC tumors with variable NE features

a, IHC of ASCL1, CD4 and CD8 in selected tumors. SCLC-04 is a SCLC tumor with NE score of 0.4. CD8 or CD4 T cells were few in the ASCL1-high regions but abundant in the ASCL1-low region; SCLC-20 is a tumor with NE score of -0.05, similar reciprocal relationship of ASCL1 staining and T cell infiltration was observed. Representative regions with high or low ASCL1 staining were shown. **b**, Relationship between IHC-determined per area CD4 and CD8 T cell count, gene expression-based T cell score and NE score in all 9 tumors assessed. Scatter plots and Pearson correlation coefficients were provided for assessment of pairwise correlations. *, Pearson correlation with p-value < 0.05. **c**, Schematic diagram showing relationship between neuroendocrine and immune gene expression in normal cells and neuroendocrine tumors (NETs).

Figure 5 Relationship between NE scores and immune phenotypes in pan-cancer samples

a-**b**, NE scores of pan-cancer samples in the TARGET pediatric cancer cohorts (**a**) and TCGA adult cancer cohorts (**b**). **c**, NE scores by immune subtype in TCGA pan-cancer samples. **d**, Relationship between NE scores and tumor-infiltrating lymphocytes regional fraction or leukocyte fraction in TCGA pan-cancer samples. **e**, Heatmap visualizing expression of various genes and summary scores previously assessed for SCLC and now in NBL with cell line and tumor datasets side-by-side. **f**, Scatter plots showing negative correlation between NE score and Ser536 phosphorylation on NFkB-p65 in NBL cell lines. Pearson correlation coefficient was provided. *, p-value < 0.05.

Figure 6 MHC I upregulation in chemoresistant SCLC

a, Heatmap visualizing increased expression of ISGs, MHC I genes as cells switch from Ascl1+ to Yap1+ in SCLC GEMM tumors from the "Lim_2017" . GFP was expressed from endogenous promoter of a Notch target gene *Hes1* in $Rb^{-/-}/p53^{-/-}/p130^{-/-}$ (TKO) background. Using flow cytometry, the authors first sorted out SCLC tumor cells and then further sorted by GFP to obtain relatively pure tumor cells with different Notch activation status. Three biological replicates were each provided for GFP negative (Notch inactive, classic high-NE) cells and GFP positive cells (Notch active, low-NE). **b**, Different morphology and culture characteristics of adherent H69-AD and the parental H69. **c**, Dose response curves for Cisplatin and Etoposide in the H69 cell line pair. Note that H69-AD, the adherent line, is more resistant with higher IC50s. **d**, Expression changes of selected genes in: H69 cell line pair from this study, H69 and derived mesenchymal H69M cell lines from "Canadas_2014" and autologous PDX samples before and after chemotherapy from "Drapkin_2018". PDX parameters: TTP, time to progression, defined by time to 2x initial tumor volume; RESP, change in tumor volume between initial tumor volume and minimum of day 14-28. Relapsed sample from MGH-1514 did not show increased chemoresistance based on the RESP and TTP parameters. Note that unlike other heatmaps, due to the small number of samples in each dataset, expression is not scaled by gene in this heatmap. **e**, qPCR measurement of normalized *ASCL1*, *B2M* and *PSMB8* expression in naïve parental and chemoresistant H1436 xenograft tumors.

SUPPLEMENTARY FIGURE LEGENDS

Figure S1 Gene ontology analyses of genes associated with NE scores in SCLC datasets

Treemaps summarizing enriched Biological Process GO terms, with reduced redundancy, for genes associated with NE scores in SCLC tumor dataset "George_2015" (**a** and **c**) or in SCLC cell lines (**b** and **d**).

Figure S2 Expression of SPARCS, parainflammation and SASP genes in SCLC datasets

a, Heatmaps visualizing expression of selected immune gene sets in multiple SCLC datasets. These gene sets were previously reported in different studies to express cell autonomously in cancer. Genes within each gene set were ordered by correlation with NE score from meta-analysis of all datasets. Gene expression matrix of each dataset was annotated with a left-side column with color-coded Pearson correlation

coefficient (from correlating NE score with gene expression), and a top bar indicating NE scores. **b**, UpSet plot showing gene counts in intersections of the three gene sets used in (**a**). SPARCS genes are genes with stimulated 3 prime antisense retroviral coding sequences; these genes have been shown to activate IFN-mediated innate immune pathways (35). Parainflammation genes are innate immunity genes that were found to express in cancer (36). SASP genes are senescence-associated secretory phenotype genes (65).

Figure S3 Repression of viral defense/hijacked genes in PNECs compared to other lung epithelial cell types

a, Violin plots showing expression of selected lineage factor (*ASCL1* and *YAP1*) and ISGs (*TLR3* and *IFI44*) in healthy human lung epithelial cells based on scRNA-seq experiments from "Travaglini_2020". Note that from research of Zika virus, *TLR3* has been shown to mediate the deleterious effect of Zika virus through disruption of neurogenesis (66). **b**, Scatter plot showing relationship among selected lineage factor genes (*Ascl1* and *Yap1*) and ISGs (*Ly6e* and *Tmprss2*) in scRNA-seq data ("Ouadah_2019") of lung epithelial cells isolated from a mouse model genetically engineered to enable lineage tracing of PNECs. AT2 and ciliated cells transdifferentiated from PNECs have lost expression of *Ascl1* but upregulated *Yap1*, *Ly6e* and *Tmprss2*. Note that from research of coronavirus, *LY6E* is implicated in viral defense (42) whereas *TMPRSS2* mediates viral entry *(43)*.

Figure S4 Expression of MHC I gene is positively associated with pan-leukocyte marker CD45 (encoded by *PTPRC*) in lung tumors and SCLC tumors

a, Expression of MHC I genes and *PTPRC* in lung tumors from Expression Project for Oncology (expO). **b**, Positive correlation between MHC I expression scores and *PTPRC* in SCLC tumors but not cell lines or PDXs ("Drapkin_2018"). *, p-value < 0.05.

Figure S5 Upregulation of immunosuppressive genes in low NE-score SCLC tumors

a, Correlation between CD274 (PD-L1) expression and NE score. Negative association was not observed in SCLC cell line or PDX ("Drapkin_2018") datasets but was observed in SCLC tumor datasets as well as NBL cell line (CCLE_neuroblastoma) and tumor (TARGET_NB) datasets. *, Pearson correlation with p-value <

0.05. **b**, Ridgeline plot showing distribution of Pearson correlation coefficients from correlating NE score to expression of 995 immunosuppressive genes (47) in SCLC cell line, PDX and patient tumor datasets. With meta-analysis in the four SCLC tumor datasets, 562 out of the 995 genes were found to have significant correlation with NE score and about 80% of those are negative correlations.

Figure S6 Cancer type-specific association between NE score and immune cell fractions

Cancer type-specific scatter plots of NE scores with tumor-infiltrating lymphocytes regional fraction (**a**) or leukocyte fraction (**b**) estimated by Thorsson, Gibbs, et al. (51) in TCGA samples.

Figure S7 Expression of *MYC* and MHC I genes (summarized as MHC I scores) in SCLC cell lines derived from primary lung tumors and metastatic tumors.

a, Scatterplots of MHC I score and *MYC* expression in lung cancer cell lines by samples types and anatomical sites of origin. **b**, MYC and MHC I gene expression score compared by anatomical site. For each gene, p-values for pairwise comparisons were calculated based on two-sided t-test followed by adjustment for multiple comparisons using the Bonferroni method.

SUPPLEMENTARY TABLES

Table S1 NE signature based on SCLC cell line RNA-seq data

Table S2 Patient characteristics, data availability and quantification of CD4 and CD8 T cells based on IHC

Table S3 Correlation between 995 immunosuppressive genes and NE scores from SCLC datasets

METHODS

Computation of NE score

The construction of the original NE signature has been described by Zhang, Girard et al.(22). In this study this signature has been updated with expression data from RNA-seq experiments. A quantitative NE score can be generated from this signature using the formula: NE score = (correl NE – correl non-NE)/2 where correl NE (or non-NE) is the Pearson correlation between expression of the 50 genes in the test sample and

expression of these genes in the NE (or non-NE) cell line group. This score has a range of −1 to +1, where a positive score predicts for NE while a negative score predicts for non-NE cell types. The higher the score in absolute value, the better the prediction.

Pathway enrichment analysis with GO terms

Gene Ontology enRIchment anaLysis and visuaLizAtion tool (GOrilla (67), http://cbl-gorilla.cs.technion.ac.il/) was used to identify enriched GO terms (68) related to biological processes (BP) from gene lists ranked by increasing or decreasing Pearson correlation with NE scores in cell line datasets or "George_2015" tumor dataset. P-value threshold was set at 10^-3 for resulting GO terms. The output was visualized by Treemap R scripts generated from "reduce + visualize gene ontology" (REViGO (69), http://revigo.irb.hr/) and further customized with modified color scheme.

Gene Set Enrichment Analysis (GSEA)

Gene set libraries were downloaded from Enrichr (24) (https://amp.pharm.mssm.edu/Enrichr/). Fast GSEA based on gene label permutation from R package "fgsea" (70) was first used for a fast screening across a large number of gene set libraries. After reviewing the results for SCLC cell lines, sample label permutation-based GSEA (23) was run for selected gene set libraries to obtain normalized enrichment scores and multiple comparison adjusted p-values. Pearson correlation was used as the ranking metric from correlating gene expression with NE scores.

Visualization

All heatmaps were generated by R package "ComplexHeatmap"(71). Other R packages used for visualization include "ggplot2" (72), "ggridges" (73), "ggrepel" (74), "ggpubr" (75), "treemap" (76), "RColorBrewer" (77), "jcolors" (78) and "patchwork" (79).

Expression data

. Drapkin_2018 (54) was downloaded from GEO with accession id GSE110853; Rudin_2012 (9) was obtained from the authors; George_2015 (10) was obtained from a supplementary table of the original

publication; Jiang_2016 (62) was downloaded from GEO with accession id GSE60052; IGC's Expression Project for Oncology - expO (GSE2109) and Rousseaux_2013 (GSE30219) (64) was processed previously for the lung cancer explorer (LCE) (63). Pan-cancer data from TCGA and TARGET was downloaded from Toil xena hub (50). For data from GEO, R package GEOquery (80) was used for extracting the expression and phenotype data. Quantile normalization was performed for bulk expression data by running the "normalize.quantiles" function from R package "preprocessCore" (81). Library size normalization was performed for author-processed scRNA-seq data by running the "library.size.normalize" function from R package "phateR" (82). Travaglini_2020 (39) was downloaded from Synapse with accession id syn21041850. FACS-sorted SmartSeq2 data was used. Cell types with less than 10 cells were removed from analyses.

Gene Signatures

SPARCS gene set is from a study by Cañadas et al (Figure 1S in original article) (35). Parainflammation gene set is from a study by Aran et al (Figure 1C in original article) (36). SASP gene set is from a study by Ruscetti et al (Figure 2C in original article) (65).

Gene set "REST ENCODE" is from the "ENCODE_and_ChEA_Consensus_TFs_from_ChIP-X" library; and "IFNA-BT2" and "IFNG-BT2" are from the "LINCS_L1000_Ligand_Perturbations_up" library. Both libraries were downloaded from Enrichr (24). Top 25 genes from leading edge and are common to all SCLC datasets were selected for heatmap visualization. For ISGs, the leading edge genes from "IFNA-BT2" and "IFNG-BT2" were first combined and then the top 25 genes were selected.

Mouse ISGs, from Cilloniz et al. (83), was identified from interferome (84) by specifying "mouse" as the species of interest and "lung" as the organ of interest. An unfiltered ISG set was used for Figure 6A.

Human MHC I gene set is a combination of genes under GO terms "GO_MHC_CLASS_I_PROTEIN_COMPLEX" and "GO_MHC_CLASS_I_PEPTIDE_LOADING_COMPLEX" from Molecular Signatures Database (MSigDB) (23, 85). Mouse MHC I genes were selected from GO:

0019885, “antigen processing and presentation of endogenous peptide antigen via MHC class I” based on the Mouse Genome Informatics (MGI) database (86). Immune-cell-specific gene sets in human are from DisHet (45). Interferon-gamma signature that predicts response to PD-1 blockade is from Ayers et al. (46). The 21-gene immune checkpoint set and 995-gene immunosuppressive set are from HisgAtlas, a human immunosuppression gene database (47).

MHC I and Immune infiltrate scores

R package GSVA (87) was used to compute immune infiltrate scores by single sample GSEA (ssGSEA) method (23, 44).

Patients and tissue specimens

Study participants included 18 patients who were diagnosis with SCLC and underwent surgical resection of lung cancer between 2006 and 2010 at the Department of Lung Cancer Surgery, Tianjin Medical University General Hospital. Written informed consent was obtained, and the institutional ethics committee of Tianjin Medical University General Hospital approved the study. The cases were selected based on the following criteria: (1) diagnosis of primary lung cancer clinical stage I to IV (pTNM); (2) undergoing surgical resection. Pathologic diagnosis was based on WHO criteria. Lung cancer staging for each patient was performed according to the AJCC Cancer Staging Manual, 8th edition, and was based on findings from physical examination, surgical resection, and computed tomography of the chest, abdomen, pelvis, and brain. The following information was collected from the patients' medical records: age, gender, clinical stage, pathologic diagnosis, differentiation, lymph node status, metastasis, smoking status, and overall survival time. Resected lung and lymph node tissues were immediately immersed in liquid nitrogen until RNA extraction.

Immunohistochemistry - histology and immunohistochemistry

Tissue blocks, once collected, were reviewed by staff thoracic pathologist to confirm SCLC histology. Consecutive four-micrometer-thick tissue sections were cut for immunohistochemistry. IHC staining was performed with a Bond Max automated staining system (Leica Microsystems Inc., Vista, CA) using IHC

parameters optimized previously. Antibodies used in this study included ASCL1 (dilution 1:25; Clone 24B72D11.1, BD Biosciences, Catalog # 556604), NEUROD1 (dilution 1:100; Clone EPR20766, Abcam, ab213725), POU2F3 (dilution 1:200; polyclonal, Novus Biologicals, NBP1-83966), CD4 (dilution 1:80; Leica Biosystems, CD4-368-L-CE-H) and CD8 (dilution 1:25; Thermo Scientific, MS-457s) in a Leica Bond Max automated stainer (Leica Biosystems Nussloch GmbH). The expression of proteins was detected using the Bond Polymer Refine Detection kit (Leica Biosystems, Cat# DS9800) with diaminobenzidine as chromogen (88). The slides were counterstained with hematoxylin, dehydrated and cover-slipped. FFPE cell lines pellets with known expression of ASCL1, NEUROD1 and POU2F3 were used to establish and optimize IHC conditions and assess sensitivity and specificity for each antibody.

Immunohistochemistry - Image analysis

The stained slides were digitally scanned using the Aperio ScanScope Turbo slide scanner (Leica Microsystems Inc.) under × 200 magnification. The images were visualized by ImageScope software (Leica Microsystems, Inc.) and analyzed using the Aperio Image Toolbox (Leica Microsystems Inc.). Different intensity levels of ASCL1, NEUROD1 or POU2F3 nuclear expression were quantified using a 4-value intensity score (0, none; 1, weak; 2, moderate; and 3, strong) and the percentage (0-100%) of the extent of reactivity. A final expression score (H-score) was obtained by multiplying the intensity and reactivity extension values (range, 0–300) as previously described (89).

The lymphocyte cells expressing CD4+ and CD8+ were counted by a pathologist using Aperio Image Toolbox analysis software (Aperio, Leica Biosystems) and expressed as cell density (CD4+ and CD8+ cells/mm^2 of analyzed tissue) (88, 90).

Microarray Assay

The Human Genome U133 Plus 2.0 microarray with 54,000 probe sets was purchased from the Affymetrix (Lot #: 4032359). Total RNA was extracted with the Trizol reagent (Invitrogen) from the tissue samples. The extracted RNA was purified using the Oligotex mRNA Midi kit (Qiagen). Then double-strand cDNA synthesis was made using one-cycle cDNA synthesis kit (Affymetrix) and purified again by column followed by the synthesis of complementary RNA (cRNA) with in vitro transcription (IVT) kit (Affymetrix). The cRNA was

fragmented after purification by column and the quality was verified by ultraviolet spectrophotometer and 1.2% denaturing agarose gel. After the test gene-chip (Lot#: 4020852, Affymetrix) was affirmed satisfactory, the real chip hybridization of cRNA fragmentation was performed and then stained and washed. Finally the real chip was scanned in Affymetrix scanner and the data was collected by GCOS (gene-chip operation software). CEL files were read into an AffyBatch object by "AffyBatch" function under the "affy" (91) R package. Alternative cdf package (92) "hgu133plus2hsentrezg" was downloaded from "http://mbni.org/customcdf/22.0.0/entrezg.download/hgu133plus2hsentrezg.db_22.0.0.zip" and was specified in the function so that the resulting expression data was processed to gene level rather than the original probe level. (Probe name follows format concatenating Entrez ID for the gene and "_at". For example "3939_at" corresponds to gene *LDHA*). The AffyBatch object was then converted to an expression set using robust multi-array average (RMA) expression measure by running the "rma" function under R package "affy". Quantile normalization was performed by running "normalize.quantiles" function from R package "preprocessCore" (81)

RNA-seq

RNA samples from SCLC cell lines (n = 69) were prepared at UT Southwestern (Dallas TX) and sent to Baylor College of Medicine (David Wheeler, Houston TX) for paired-end RNA sequencing. Analysis was then performed at UT Southwestern: Reads were aligned to the human reference genome GRCh38 using STAR-2.7(93) (https://github.com/alexdobin/STAR) and FPKM values were generated with cufflinks-2.2.1 (94) (http://cole-trapnell-lab.github.io/cufflinks/). All data were then pooled, upper-quartile normalized (95), and log-transformed.

Cell culture

All SCLC cell lines used in these studies were originally established in the John D. Minna and Adi F. Gazdar laboratories. The cultured Small Cell Lung Cancer (SCLC) cell lines were obtained from both the National Cancer Institute (NCI) and Hamon Cancer Center (HCC) libraries. Cells were cultured in RPMI-1640 media (Sigma Life Science, St. Louis, MO) supplemented with 5% Fetal Bovine Serum (FBS). RPMI-1640 supplemented with 5% FBS will be referred to as R5. All cells were incubated in NuAire (NuAire, Plymouth,

MN) humidified incubators at 37°C at 5% CO2. All cell lines were regularly tested for mycoplasma contamination (Bulldog Bio, Portsmouth, NH) and fingerprinted using a PowerPlex 1.2 kit (Promega, Madison, WI) to confirm the cell line identity.

Establishing adherent H69 (H69-AD)

The early passage of parental H69 cell line grew as a mixture of floating and adherent cells. To enrich for adherent cells, the floating population of H69 was washed off during growth media replacement and fresh media was provided for expansion of the remaining adherent cells. This was repeated until every passage grew as adherent cells with few to no suspension cells. This derived adherent subline was designated as H69-AD.

Drug response assay

Cisplatin and Etoposide were obtained from Selleck Chemicals LLC, USA. 5,000 cells of H69 and H69-AD were cultured in 100 uL R5 growth media per well in ultra-low adherent, clear, round bottom, 96 well plates (BD Biosciences, USA) for 48 hours. An additional 100 µl R5 plus either a control (DMSO) or drug was added to the plate. 96 hours after drug treatment, each cell line was assayed using the Cell-Titer-Glo reagent (Promega, Inc.). The fluorescence intensity was recorded at 570 nM. A standard 4-parameter log-logistic fit between the survival rate and the dosage was generated by the ‘‘drm’’ function from the R package ‘‘drc’’(96).

Xenograft models for parental and chemoresistant SCLC tumors

Subcutaneous xenograft in NSG mice was derived from direct implantation of untreated H1436 cells or re-implantation of chemoresistant tumors after 4 cycles of Cisplatin and Etoposide (EC), or plus 4 cycles of Cisplatin (reduced from EC due to toxicity). Specifically, a million H1436 cells were resuspended in 100 µl mixture of serum-free RPMI 1640 and Matrigel (BD Bioscience #356237) at 1:1 ratio and immediately injected in the flank of 6-8-week-old female NSG mouse (Jackson Laboratory #005557). Mice were randomized after tumor cell injection. Treatment starts after a week when the tumor becomes palpable. 5 mg/kg/w Cisplatin (Sigma P4394) in saline, 10 mg/kg/w Etoposide (Sigma E1383) in 30% PEG 300 (Sigma

202371) were freshly prepared and administered by intraperitoneal injection, for 4 cycles in total to obtain the first group of chemoresistant tumors. An additional 4 cycles of Cisplatin were administered in a second group of mice to obtain tumors with further potentiated chemoresistance. To harvest the tumor, 10 ml digestion media was used per mouse. This was prepared freshly by supplementing 9 ml HBSS with 1 ml type IV collagenase, 50 µl DNase II and 50 µl 1 M $CaCl_2$. Tumors were collected and placed in HBSS immediately following dissection. A fraction of the tumor was cut into a few pieces and flash-frozen in liquid nitrogen to be saved in aliquots for molecular assays. The remaining chunk was finely minced with a sterile scalpel blade. For re-implantation, the minced tissue was resuspended in digestion media, rotated at 37 °C for 20 min, filtered through a 40 µm filter, centrifuged at 300x g for 5 min.

Quantitative reverse transcription PCR

~20 mg flash-frozen tumor fragments were weighed out and homogenized in 1 ml TRIzol (Invitrogen #15596-026) in Precellys tissue homogenizing mixed beads kit (Cayman Chemical #10409). 0.2 ml chloroform (Fisher #S25248) was added to the TRIzol lysate and the mixture was vortexed for 10 s and centrifuged at 12,000 x g for 15 min at 4 °C for phase separation. 450 ul aqueous phase was collected, mixed well with 0.5 ml isopropanol (Fisher #A451-1) and precipitated RNA was collected by centrifugation at 12,000 x g for 10 min at 4 °C, The RNA pellet was rinsed in 1 ml 75% ethanol, then dissolved in 100 µl deionized water by incubating at 55 °C for 5 min. 500 ng total RNA was reverse-transcribed to cDNA in a 20 µl reaction with 4 µl iScript reverse transcription supermix (Bio-Rad #1708841) at 25 °C for 5 min, 46 °C for 20 min, and 95 °C for 1 min. The mixture was then 1:5 diluted with deionized water. Target sequences in cDNA library were amplified in 10 µl qPCR reaction (5 µl SYBR Green supermix (Bio-Rad #1725121), 0.675 µl 2.5 µM primer mix and 0.45 µl diluted cDNA) at 95 °C 10 s, 60 °C 30 s, for 40 cycles. All procedures were performed under RNase-free condition unless specified. For data analysis, median was taken from triplicates, normalized by Ct values of control gene *PPIA*, exponentiated with base 2 then divided by the median of parental samples.

Study Approval

The protocol of collecting human SCLC tumor tissue for research was approved by the Ethics Committee of Tianjin Medical University General Hospital. Written informed consent was received from participants prior to inclusion in the study. Specimen collection did not interfere with standard diagnostic and therapeutic procedures. All mouse procedures were performed with the approval of the University of Texas Southwestern Medical Center IACUC.

Data availability

Scripts used for this manuscript are available upon request. The RNA-seq gene expression data from UTSW SCLC has been added to dbGaP (accession phs001823.v1.p1) (97). SCLC tumor microarray data used in this study has been deposited to GEO with accession id GSE149507.

ACKNOWLEDGEMENT

Support for this work comes from the National Institutes of Health [1R35GM136375, 5P30CA142543, 5U01CA213338-04, 3P50CA070907, and R01GM115473], and the Cancer Prevention Research Institute of Texas [RP180805]. We dedicate this work to Dr. Adi F. Gazdar, who had initially conceptualized and led this project until his passing in December 2018. We thank Ms. Jessie Norris for proofreading the manuscript.

AUTHOR CONTRIBUTIONS

Conception and design, A.F.G. and L.C.; Development of methodology, L.C., L.G. and T.W.; Acquisition of data, L.C., H.L., F.H., J.F., L.G., J.C., Y.L., Y.Z., D.D., V.S., C.S.K., C.Y., A.A., K.H., M.P. and B.D.; Analysis and interpretation of data, L.C., J.F., G.J., L.Y. and W.Z.; Writing, review and/or revision of the manuscript, L.C., H.L., E.A., R.J.D and J.D.M.; Study supervision, D.S.S., I.I.W., G.X., J.D.M., Y.X. and A.F.G.

COMPETING INTERESTS

J.D.M. receives licensing fees from the NCI and UT Southwestern to distribute cell lines. R.J.D is on the advisory board for Agios Pharmaceuticals. D.S.S and W.Z. are currently employed by Genentech Inc. and own stock in Roche Holdings. I.I.W is speaker at Medscape, MSD, Genentech/Roche, PlatformQ Health,

Pfizer, AstraZeneca, Merck; receives research support from Genentech, Oncoplex, HTG Molecular, DepArray, Merck, Bristol-Myers Squibb, Medimmune, Adaptive, Adaptimmune, EMD Serono, Pfizer, Takeda, Amgen, Karus, Johnson & Johnson, Bayer, Iovance, 4D, Novartis, and Akoya; and is on the advisory boards for Genentech/Roche, Bayer, Bristol-Myers Squibb, AstraZeneca/Medimmune, Pfizer, HTG Molecular, Asuragen, Merck, GlaxoSmithKline, Guardant Health, Oncocyte, and MSD.

REFERENCE

1. Gazdar AF, Bunn PA, Minna JD. Small-cell lung cancer: what we know, what we need to know and the path forward. Nat Rev Cancer. 2017;17(12):765. Epub 2017/11/11. doi: 10.1038/nrc.2017.106. PubMed PMID: 29123245.
2. H.R.733 UC. Recalcitrant Cancer Research Act of 2012 2012. Available from: https://www.congress.gov/bill/112th-congress/house-bill/733.
3. Travis WD, Brambilla E, Nicholson AG, Yatabe Y, Austin JHM, Beasley MB, Chirieac LR, Dacic S, Duhig E, Flieder DB, Geisinger K, Hirsch FR, Ishikawa Y, Kerr KM, Noguchi M, Pelosi G, Powell CA, Tsao MS, Wistuba I, Panel WHO. The 2015 World Health Organization Classification of Lung Tumors: Impact of Genetic, Clinical and Radiologic Advances Since the 2004 Classification. J Thorac Oncol. 2015;10(9):1243-60. Epub 2015/08/21. doi: 10.1097/JTO.0000000000000630. PubMed PMID: 26291008.
4. Augustyn A, Borromeo M, Wang T, Fujimoto J, Shao C, Dospoy PD, Lee V, Tan C, Sullivan JP, Larsen JE, Girard L, Behrens C, Wistuba, II, Xie Y, Cobb MH, Gazdar AF, Johnson JE, Minna JD. ASCL1 is a lineage oncogene providing therapeutic targets for high-grade neuroendocrine lung cancers. Proc Natl Acad Sci U S A. 2014;111(41):14788-93. Epub 2014/10/01. doi: 10.1073/pnas.1410419111. PubMed PMID: 25267614; PMCID: PMC4205603.
5. Borges M, Linnoila RI, van de Velde HJ, Chen H, Nelkin BD, Mabry M, Baylin SB, Ball DW. An achaete-scute homologue essential for neuroendocrine differentiation in the lung. Nature. 1997;386(6627):852-5. Epub 1997/04/24. doi: 10.1038/386852a0. PubMed PMID: 9126746.
6. Boers JE, den Brok JL, Koudstaal J, Arends JW, Thunnissen FB. Number and proliferation of neuroendocrine cells in normal human airway epithelium. Am J Respir Crit Care Med. 1996;154(3 Pt 1):758-63. Epub 1996/09/01. doi: 10.1164/ajrccm.154.3.8810616. PubMed PMID: 8810616.
7. Ouadah Y, Rojas ER, Riordan DP, Capostagno S, Kuo CS, Krasnow MA. Rare Pulmonary Neuroendocrine Cells Are Stem Cells Regulated by Rb, p53, and Notch. Cell. 2019;179(2):403-16 e23. Epub 2019/10/05. doi: 10.1016/j.cell.2019.09.010. PubMed PMID: 31585080; PMCID: PMC6782070.
8. Pleasance ED, Stephens PJ, O'Meara S, McBride DJ, Meynert A, Jones D, Lin ML, Beare D, Lau KW, Greenman C, Varela I, Nik-Zainal S, Davies HR, Ordonez GR, Mudie LJ, Latimer C, Edkins S, Stebbings L, Chen L, Jia M, Leroy C, Marshall J, Menzies A, Butler A, Teague JW, Mangion J, Sun YA, McLaughlin SF, Peckham HE, Tsung EF, Costa GL, Lee CC, Minna JD, Gazdar A, Birney E, Rhodes MD, McKernan KJ, Stratton MR, Futreal PA, Campbell PJ. A small-cell lung cancer genome with complex signatures of tobacco exposure. Nature. 2010;463(7278):184-90. Epub 2009/12/18. doi: 10.1038/nature08629. PubMed PMID: 20016488; PMCID: PMC2880489.
9. Rudin CM, Durinck S, Stawiski EW, Poirier JT, Modrusan Z, Shames DS, Bergbower EA, Guan Y, Shin J, Guillory J, Rivers CS, Foo CK, Bhatt D, Stinson J, Gnad F, Haverty PM, Gentleman R, Chaudhuri S, Janakiraman V, Jaiswal BS, Parikh C, Yuan W, Zhang Z, Koeppen H, Wu TD, Stern HM, Yauch RL, Huffman KE, Paskulin DD, Illei PB, Varella-Garcia M, Gazdar AF, de Sauvage FJ, Bourgon R, Minna JD, Brock MV, Seshagiri S. Comprehensive genomic analysis identifies SOX2 as a frequently amplified gene

740 in small-cell lung cancer. Nat Genet. 2012;44(10):1111-6. Epub 2012/09/04. doi: 10.1038/ng.2405.
741 PubMed PMID: 22941189; PMCID: PMC3557461.
742 10. George J, Lim JS, Jang SJ, Cun Y, Ozretic L, Kong G, Leenders F, Lu X, Fernandez-Cuesta L, Bosco
743 G, Muller C, Dahmen I, Jahchan NS, Park KS, Yang D, Karnezis AN, Vaka D, Torres A, Wang MS, Korbel
744 JO, Menon R, Chun SM, Kim D, Wilkerson M, Hayes N, Engelmann D, Putzer B, Bos M, Michels S, Vlasic I,
745 Seidel D, Pinther B, Schaub P, Becker C, Altmuller J, Yokota J, Kohno T, Iwakawa R, Tsuta K, Noguchi M,
746 Muley T, Hoffmann H, Schnabel PA, Petersen I, Chen Y, Soltermann A, Tischler V, Choi CM, Kim YH,
747 Massion PP, Zou Y, Jovanovic D, Kontic M, Wright GM, Russell PA, Solomon B, Koch I, Lindner M,
748 Muscarella LA, la Torre A, Field JK, Jakopovic M, Knezevic J, Castanos-Velez E, Roz L, Pastorino U,
749 Brustugun OT, Lund-Iversen M, Thunnissen E, Kohler J, Schuler M, Botling J, Sandelin M, Sanchez-
750 Cespedes M, Salvesen HB, Achter V, Lang U, Bogus M, Schneider PM, Zander T, Ansen S, Hallek M, Wolf
751 J, Vingron M, Yatabe Y, Travis WD, Nurnberg P, Reinhardt C, Perner S, Heukamp L, Buttner R, Haas SA,
752 Brambilla E, Peifer M, Sage J, Thomas RK. Comprehensive genomic profiles of small cell lung cancer.
753 Nature. 2015;524(7563):47-53. Epub 2015/07/15. doi: 10.1038/nature14664. PubMed PMID:
754 26168399; PMCID: PMC4861069.
755 11. Doyle A, Martin WJ, Funa K, Gazdar A, Carney D, Martin SE, Linnoila I, Cuttitta F, Mulshine J,
756 Bunn P, et al. Markedly decreased expression of class I histocompatibility antigens, protein, and mRNA
757 in human small-cell lung cancer. J Exp Med. 1985;161(5):1135-51. Epub 1985/05/01. doi:
758 10.1084/jem.161.5.1135. PubMed PMID: 2580935; PMCID: PMC2187608.
759 12. Burr ML, Sparbier CE, Chan KL, Chan YC, Kersbergen A, Lam EYN, Azidis-Yates E, Vassiliadis D,
760 Bell CC, Gilan O, Jackson S, Tan L, Wong SQ, Hollizeck S, Michalak EM, Siddle HV, McCabe MT, Prinjha
761 RK, Guerra GR, Solomon BJ, Sandhu S, Dawson SJ, Beavis PA, Tothill RW, Cullinane C, Lehner PJ,
762 Sutherland KD, Dawson MA. An Evolutionarily Conserved Function of Polycomb Silences the MHC
763 Class I Antigen Presentation Pathway and Enables Immune Evasion in Cancer. Cancer Cell.
764 2019;36(4):385-401 e8. Epub 2019/10/01. doi: 10.1016/j.ccell.2019.08.008. PubMed PMID:
765 31564637; PMCID: PMC6876280.
766 13. Yarchoan M, Hopkins A, Jaffee EM. Tumor Mutational Burden and Response Rate to PD-1
767 Inhibition. N Engl J Med. 2017;377(25):2500-1. Epub 2017/12/21. doi: 10.1056/NEJMc1713444.
768 PubMed PMID: 29262275; PMCID: PMC6549688.
769 14. Iams WT, Porter J, Horn L. Immunotherapeutic approaches for small-cell lung cancer. Nat Rev
770 Clin Oncol. 2020. Epub 2020/02/15. doi: 10.1038/s41571-019-0316-z. PubMed PMID: 32055013.
771 15. Gazdar AF, Carney DN, Nau MM, Minna JD. Characterization of variant subclasses of cell lines
772 derived from small cell lung cancer having distinctive biochemical, morphological, and growth
773 properties. Cancer Res. 1985;45(6):2924-30. Epub 1985/06/01. PubMed PMID: 2985258.
774 16. Carney DN, Gazdar AF, Bepler G, Guccion JG, Marangos PJ, Moody TW, Zweig MH, Minna JD.
775 Establishment and identification of small cell lung cancer cell lines having classic and variant features.
776 Cancer Res. 1985;45(6):2913-23. Epub 1985/06/01. PubMed PMID: 2985257.
777 17. Johnson BE, Russell E, Simmons AM, Phelps R, Steinberg SM, Ihde DC, Gazdar AF. MYC family
778 DNA amplification in 126 tumor cell lines from patients with small cell lung cancer. J Cell Biochem
779 Suppl. 1996;24:210-7. Epub 1996/01/01. doi: 10.1002/jcb.240630516. PubMed PMID: 8806103.
780 18. Lim JS, Ibaseta A, Fischer MM, Cancilla B, O'Young G, Cristea S, Luca VC, Yang D, Jahchan NS,
781 Hamard C, Antoine M, Wislez M, Kong C, Cain J, Liu YW, Kapoun AM, Garcia KC, Hoey T, Murriel CL,
782 Sage J. Intratumoural heterogeneity generated by Notch signalling promotes small-cell lung cancer.
783 Nature. 2017;545(7654):360-4. Epub 2017/05/11. doi: 10.1038/nature22323. PubMed PMID:
784 28489825; PMCID: PMC5776014.
785 19. Gazdar AF, Bunn PA, Minna JD. Small-cell lung cancer: what we know, what we need to know
786 and the path forward. Nat Rev Cancer. 2017;17(12):725-37. doi: 10.1038/nrc.2017.87. PubMed PMID:
787 29077690.
788 20. Rudin CM, Poirier JT, Byers LA, Dive C, Dowlati A, George J, Heymach JV, Johnson JE, Lehman JM,
789 MacPherson D, Massion PP, Minna JD, Oliver TG, Quaranta V, Sage J, Thomas RK, Vakoc CR, Gazdar AF.

790 Molecular subtypes of small cell lung cancer: a synthesis of human and mouse model data. Nat Rev
791 Cancer. 2019;19(5):289-97. Epub 2019/03/31. doi: 10.1038/s41568-019-0133-9. PubMed PMID:
792 30926931; PMCID: PMC6538259.
793 21. Gazdar AF. Morphologic and Other Forms of Heterogeneity in Small Cell Lung Cancer: What Can
794 We Learn from Them? J Thorac Oncol. 2018;13(2):148-50. Epub 2018/02/10. doi:
795 10.1016/j.jtho.2017.11.004. PubMed PMID: 29425612.
796 22. Zhang W, Girard L, Zhang YA, Haruki T, Papari-Zareei M, Stastny V, Ghayee HK, Pacak K, Oliver
797 TG, Minna JD, Gazdar AF. Small cell lung cancer tumors and preclinical models display heterogeneity of
798 neuroendocrine phenotypes. Transl Lung Cancer Res. 2018;7(1):32-49. Epub 2018/03/15. doi:
799 10.21037/tlcr.2018.02.02. PubMed PMID: 29535911; PMCID: PMC5835590.
800 23. Subramanian A, Tamayo P, Mootha VK, Mukherjee S, Ebert BL, Gillette MA, Paulovich A,
801 Pomeroy SL, Golub TR, Lander ES, Mesirov JP. Gene set enrichment analysis: a knowledge-based
802 approach for interpreting genome-wide expression profiles. Proc Natl Acad Sci U S A.
803 2005;102(43):15545-50. Epub 2005/10/04. doi: 10.1073/pnas.0506580102. PubMed PMID:
804 16199517; PMCID: PMC1239896.
805 24. Kuleshov MV, Jones MR, Rouillard AD, Fernandez NF, Duan Q, Wang Z, Koplev S, Jenkins SL,
806 Jagodnik KM, Lachmann A, McDermott MG, Monteiro CD, Gundersen GW, Ma'ayan A. Enrichr: a
807 comprehensive gene set enrichment analysis web server 2016 update. Nucleic Acids Res.
808 2016;44(W1):W90-7. Epub 2016/05/05. doi: 10.1093/nar/gkw377. PubMed PMID: 27141961;
809 PMCID: PMC4987924.
810 25. Ghandi M, Huang FW, Jane-Valbuena J, Kryukov GV, Lo CC, McDonald ER, 3rd, Barretina J,
811 Gelfand ET, Bielski CM, Li H, Hu K, Andreev-Drakhlin AY, Kim J, Hess JM, Haas BJ, Aguet F, Weir BA,
812 Rothberg MV, Paolella BR, Lawrence MS, Akbani R, Lu Y, Tiv HL, Gokhale PC, de Weck A, Mansour AA,
813 Oh C, Shih J, Hadi K, Rosen Y, Bistline J, Venkatesan K, Reddy A, Sonkin D, Liu M, Lehar J, Korn JM,
814 Porter DA, Jones MD, Golji J, Caponigro G, Taylor JE, Dunning CM, Creech AL, Warren AC, McFarland JM,
815 Zamanighomi M, Kauffmann A, Stransky N, Imielinski M, Maruvka YE, Cherniack AD, Tsherniak A,
816 Vazquez F, Jaffe JD, Lane AA, Weinstock DM, Johannessen CM, Morrissey MP, Stegmeier F, Schlegel R,
817 Hahn WC, Getz G, Mills GB, Boehm JS, Golub TR, Garraway LA, Sellers WR. Next-generation
818 characterization of the Cancer Cell Line Encyclopedia. Nature. 2019;569(7757):503-8. doi:
819 10.1038/s41586-019-1186-3. PubMed PMID: 31068700.
820 26. Sakurai H, Chiba H, Miyoshi H, Sugita T, Toriumi W. IkappaB kinases phosphorylate NF-kappaB
821 p65 subunit on serine 536 in the transactivation domain. J Biol Chem. 1999;274(43):30353-6. Epub
822 1999/10/16. doi: 10.1074/jbc.274.43.30353. PubMed PMID: 10521409.
823 27. Dinarello CA. Interleukin-18, a proinflammatory cytokine. Eur Cytokine Netw. 2000;11(3):483-
824 6. Epub 2001/02/24. PubMed PMID: 11203186.
825 28. Cornelissen C, Luscher-Firzlaff J, Baron JM, Luscher B. Signaling by IL-31 and functional
826 consequences. Eur J Cell Biol. 2012;91(6-7):552-66. Epub 2011/10/11. doi:
827 10.1016/j.ejcb.2011.07.006. PubMed PMID: 21982586.
828 29. Kordass T, Osen W, Eichmuller SB. Controlling the Immune Suppressor: Transcription Factors
829 and MicroRNAs Regulating CD73/NT5E. Front Immunol. 2018;9:813. Epub 2018/05/04. doi:
830 10.3389/fimmu.2018.00813. PubMed PMID: 29720980; PMCID: PMC5915482.
831 30. Yang L, Pang Y, Moses HL. TGF-beta and immune cells: an important regulatory axis in the
832 tumor microenvironment and progression. Trends Immunol. 2010;31(6):220-7. Epub 2010/06/12.
833 doi: 10.1016/j.it.2010.04.002. PubMed PMID: 20538542; PMCID: PMC2891151.
834 31. D'Acquisto F, Perretti M, Flower RJ. Annexin-A1: a pivotal regulator of the innate and adaptive
835 immune systems. Br J Pharmacol. 2008;155(2):152-69. Epub 2008/07/22. doi: 10.1038/bjp.2008.252.
836 PubMed PMID: 18641677; PMCID: PMC2538690.
837 32. Markosyan N, Li J, Sun YH, Richman LP, Lin JH, Yan F, Quinones L, Sela Y, Yamazoe T, Gordon N,
838 Tobias JW, Byrne KT, Rech AJ, FitzGerald GA, Stanger BZ, Vonderheide RH. Tumor cell-intrinsic EPHA2

suppresses anti-tumor immunity by regulating PTGS2 (COX-2). J Clin Invest. 2019;130:3594-609. Epub 2019/06/05. doi: 10.1172/JCI127755. PubMed PMID: 31162144; PMCID: PMC6715369.
33. Reuben A, Chung JW, Lapointe R, Santos MM. The hemochromatosis protein HFE 20 years later: An emerging role in antigen presentation and in the immune system. Immun Inflamm Dis. 2017;5(3):218-32. Epub 2017/05/06. doi: 10.1002/iid3.158. PubMed PMID: 28474781; PMCID: PMC5569368.
34. Kouo T, Huang L, Pucsek AB, Cao M, Solt S, Armstrong T, Jaffee E. Galectin-3 Shapes Antitumor Immune Responses by Suppressing CD8+ T Cells via LAG-3 and Inhibiting Expansion of Plasmacytoid Dendritic Cells. Cancer Immunol Res. 2015;3(4):412-23. Epub 2015/02/19. doi: 10.1158/2326-6066.CIR-14-0150. PubMed PMID: 25691328; PMCID: PMC4390508.
35. Canadas I, Thummalapalli R, Kim JW, Kitajima S, Jenkins RW, Christensen CL, Campisi M, Kuang Y, Zhang Y, Gjini E, Zhang G, Tian T, Sen DR, Miao D, Imamura Y, Thai T, Piel B, Terai H, Aref AR, Hagan T, Koyama S, Watanabe M, Baba H, Adeni AE, Lydon CA, Tamayo P, Wei Z, Herlyn M, Barbie TU, Uppaluri R, Sholl LM, Sicinska E, Sands J, Rodig S, Wong KK, Paweletz CP, Watanabe H, Barbie DA. Tumor innate immunity primed by specific interferon-stimulated endogenous retroviruses. Nat Med. 2018;24(8):1143-50. Epub 2018/07/25. doi: 10.1038/s41591-018-0116-5. PubMed PMID: 30038220; PMCID: PMC6082722.
36. Aran D, Lasry A, Zinger A, Biton M, Pikarsky E, Hellman A, Butte AJ, Ben-Neriah Y. Widespread parainflammation in human cancer. Genome Biol. 2016;17(1):145. Epub 2016/07/09. doi: 10.1186/s13059-016-0995-z. PubMed PMID: 27386949; PMCID: PMC4937599.
37. Coppe JP, Patil CK, Rodier F, Sun Y, Munoz DP, Goldstein J, Nelson PS, Desprez PY, Campisi J. Senescence-associated secretory phenotypes reveal cell-nonautonomous functions of oncogenic RAS and the p53 tumor suppressor. PLoS Biol. 2008;6(12):2853-68. Epub 2008/12/05. doi: 10.1371/journal.pbio.0060301. PubMed PMID: 19053174; PMCID: PMC2592359.
38. Chien Y, Scuoppo C, Wang X, Fang X, Balgley B, Bolden JE, Premsrirut P, Luo W, Chicas A, Lee CS, Kogan SC, Lowe SW. Control of the senescence-associated secretory phenotype by NF-kappaB promotes senescence and enhances chemosensitivity. Genes Dev. 2011;25(20):2125-36. Epub 2011/10/08. doi: 10.1101/gad.17276711. PubMed PMID: 21979375; PMCID: PMC3205583.
39. Travaglini KJ, Nabhan AN, Penland L, Sinha R, Gillich A, Sit RV, Chang S, Conley SD, Mori Y, Seita J, Berry GJ, Shrager JB, Metzger RJ, Kuo CS, Neff N, Weissman IL, Quake SR, Krasnow MA. A molecular cell atlas of the human lung from single cell RNA sequencing. bioRxiv. 2019.
40. Zhang H, Deo M, Thompson RC, Uhler MD, Turner DL. Negative regulation of Yap during neuronal differentiation. Dev Biol. 2012;361(1):103-15. Epub 2011/11/01. doi: 10.1016/j.ydbio.2011.10.017. PubMed PMID: 22037235; PMCID: PMC3235039.
41. Schoggins JW. Interferon-Stimulated Genes: What Do They All Do? Annu Rev Virol. 2019;6(1):567-84. Epub 2019/07/10. doi: 10.1146/annurev-virology-092818-015756. PubMed PMID: 31283436.
42. Pfaender S, Mar KB, Michailidis E, Kratzel A, Hirt D, V'kovski P, Fan W, Ebert N, Stalder H, Kleine-Weber H, Hoffmann M, Hoffmann HH, Saeed M, Dijkman R, Steinmann E, Wight-Carter M, Hanners NW, Pöhlmann S, Gallagher T, Todt D, Zimmer G, Rice CM, Schoggins JW, Thiel V. LY6E impairs coronavirus fusion and confers immune control of viral disease. bioRxiv. 2020.
43. Shen LW, Mao HJ, Wu YL, Tanaka Y, Zhang W. TMPRSS2: A potential target for treatment of influenza virus and coronavirus infections. Biochimie. 2017;142:1-10. Epub 2017/08/06. doi: 10.1016/j.biochi.2017.07.016. PubMed PMID: 28778717; PMCID: PMC7116903.
44. Barbie DA, Tamayo P, Boehm JS, Kim SY, Moody SE, Dunn IF, Schinzel AC, Sandy P, Meylan E, Scholl C, Frohling S, Chan EM, Sos ML, Michel K, Mermel C, Silver SJ, Weir BA, Reiling JH, Sheng Q, Gupta PB, Wadlow RC, Le H, Hoersch S, Wittner BS, Ramaswamy S, Livingston DM, Sabatini DM, Meyerson M, Thomas RK, Lander ES, Mesirov JP, Root DE, Gilliland DG, Jacks T, Hahn WC. Systematic RNA interference reveals that oncogenic KRAS-driven cancers require TBK1. Nature. 2009;462(7269):108-12. Epub 2009/10/23. doi: 10.1038/nature08460. PubMed PMID: 19847166; PMCID: PMC2783335.

45. Wang T, Lu R, Kapur P, Jaiswal BS, Hannan R, Zhang Z, Pedrosa I, Luke JJ, Zhang H, Goldstein LD, Yousuf Q, Gu YF, McKenzie T, Joyce A, Kim MS, Wang X, Luo D, Onabolu O, Stevens C, Xie Z, Chen M, Filatenkov A, Torrealba J, Luo X, Guo W, He J, Stawiski E, Modrusan Z, Durinck S, Seshagiri S, Brugarolas J. An Empirical Approach Leveraging Tumorgrafts to Dissect the Tumor Microenvironment in Renal Cell Carcinoma Identifies Missing Link to Prognostic Inflammatory Factors. Cancer Discov. 2018;8(9):1142-55. Epub 2018/06/10. doi: 10.1158/2159-8290.CD-17-1246. PubMed PMID: 29884728; PMCID: PMC6125163.
46. Ayers M, Lunceford J, Nebozhyn M, Murphy E, Loboda A, Kaufman DR, Albright A, Cheng JD, Kang SP, Shankaran V, Piha-Paul SA, Yearley J, Seiwert TY, Ribas A, McClanahan TK. IFN-gamma-related mRNA profile predicts clinical response to PD-1 blockade. J Clin Invest. 2017;127(8):2930-40. Epub 2017/06/27. doi: 10.1172/JCI91190. PubMed PMID: 28650338; PMCID: PMC5531419.
47. Liu Y, He M, Wang D, Diao L, Liu J, Tang L, Guo S, He F, Li D. HisgAtlas 1.0: a human immunosuppression gene database. Database (Oxford). 2017;2017. Epub 2017/01/01. doi: 10.1093/database/bax094. PubMed PMID: 31725860.
48. Lee S, Margolin K. Cytokines in cancer immunotherapy. Cancers (Basel). 2011;3(4):3856-93. Epub 2011/01/01. doi: 10.3390/cancers3043856. PubMed PMID: 24213115; PMCID: PMC3763400.
49. Balanis NG, Sheu KM, Esedebe FN, Patel SJ, Smith BA, Park JW, Alhani S, Gomperts BN, Huang J, Witte ON, Graeber TG. Pan-cancer Convergence to a Small-Cell Neuroendocrine Phenotype that Shares Susceptibilities with Hematological Malignancies. Cancer Cell. 2019;36(1):17-34 e7. Epub 2019/07/10. doi: 10.1016/j.ccell.2019.06.005. PubMed PMID: 31287989; PMCID: PMC6703903.
50. Vivian J, Rao AA, Nothaft FA, Ketchum C, Armstrong J, Novak A, Pfeil J, Narkizian J, Deran AD, Musselman-Brown A, Schmidt H, Amstutz P, Craft B, Goldman M, Rosenbloom K, Cline M, O'Connor B, Hanna M, Birger C, Kent WJ, Patterson DA, Joseph AD, Zhu J, Zaranek S, Getz G, Haussler D, Paten B. Toil enables reproducible, open source, big biomedical data analyses. Nat Biotechnol. 2017;35(4):314-6. Epub 2017/04/12. doi: 10.1038/nbt.3772. PubMed PMID: 28398314; PMCID: PMC5546205.
51. Thorsson V, Gibbs DL, Brown SD, Wolf D, Bortone DS, Ou Yang TH, Porta-Pardo E, Gao GF, Plaisier CL, Eddy JA, Ziv E, Culhane AC, Paull EO, Sivakumar IKA, Gentles AJ, Malhotra R, Farshidfar F, Colaprico A, Parker JS, Mose LE, Vo NS, Liu J, Liu Y, Rader J, Dhankani V, Reynolds SM, Bowlby R, Califano A, Cherniack AD, Anastassiou D, Bedognetti D, Mokrab Y, Newman AM, Rao A, Chen K, Krasnitz A, Hu H, Malta TM, Noushmehr H, Pedamallu CS, Bullman S, Ojesina AI, Lamb A, Zhou W, Shen H, Choueiri TK, Weinstein JN, Guinney J, Saltz J, Holt RA, Rabkin CS, Cancer Genome Atlas Research N, Lazar AJ, Serody JS, Demicco EG, Disis ML, Vincent BG, Shmulevich I. The Immune Landscape of Cancer. Immunity. 2018;48(4):812-30 e14. Epub 2018/04/10. doi: 10.1016/j.immuni.2018.03.023. PubMed PMID: 29628290; PMCID: PMC5982584.
52. Pugh TJ, Morozova O, Attiyeh EF, Asgharzadeh S, Wei JS, Auclair D, Carter SL, Cibulskis K, Hanna M, Kiezun A, Kim J, Lawrence MS, Lichenstein L, McKenna A, Pedamallu CS, Ramos AH, Shefler E, Sivachenko A, Sougnez C, Stewart C, Ally A, Birol I, Chiu R, Corbett RD, Hirst M, Jackman SD, Kamoh B, Khodabakshi AH, Krzywinski M, Lo A, Moore RA, Mungall KL, Qian J, Tam A, Thiessen N, Zhao Y, Cole KA, Diamond M, Diskin SJ, Mosse YP, Wood AC, Ji L, Sposto R, Badgett T, London WB, Moyer Y, Gastier-Foster JM, Smith MA, Guidry Auvil JM, Gerhard DS, Hogarty MD, Jones SJ, Lander ES, Gabriel SB, Getz G, Seeger RC, Khan J, Marra MA, Meyerson M, Maris JM. The genetic landscape of high-risk neuroblastoma. Nat Genet. 2013;45(3):279-84. Epub 2013/01/22. doi: 10.1038/ng.2529. PubMed PMID: 23334666; PMCID: PMC3682833.
53. Canadas I, Rojo F, Taus A, Arpi O, Arumi-Uria M, Pijuan L, Menendez S, Zazo S, Domine M, Salido M, Mojal S, Garcia de Herreros A, Rovira A, Albanell J, Arriola E. Targeting epithelial-to-mesenchymal transition with Met inhibitors reverts chemoresistance in small cell lung cancer. Clin Cancer Res. 2014;20(4):938-50. Epub 2013/11/29. doi: 10.1158/1078-0432.CCR-13-1330. PubMed PMID: 24284055.
54. Drapkin BJ, George J, Christensen CL, Mino-Kenudson M, Dries R, Sundaresan T, Phat S, Myers DT, Zhong J, Igo P, Hazar-Rethinam MH, Licausi JA, Gomez-Caraballo M, Kem M, Jani KN, Azimi R,

939 Abedpour N, Menon R, Lakis S, Heist RS, Buttner R, Haas S, Sequist LV, Shaw AT, Wong KK, Hata AN,
940 Toner M, Maheswaran S, Haber DA, Peifer M, Dyson N, Thomas RK, Farago AF. Genomic and Functional
941 Fidelity of Small Cell Lung Cancer Patient-Derived Xenografts. Cancer Discov. 2018;8(5):600-15. Epub
942 2018/02/28. doi: 10.1158/2159-8290.CD-17-0935. PubMed PMID: 29483136; PMCID: PMC6369413.
943 55. Ireland AS, Micinski AM, Kastner DW, Guo B, Wait SJ, Spainhower KB, Conley CC, Chen OS,
944 Guthrie MR, Soltero D, Qiao Y, Huang X, Tarapcsak S, Devarakonda S, Chalishazar MD, Gertz J, Moser JC,
945 Marth G, Puri S, Witt BL, Spike BT, Oliver TG. MYC Drives Temporal Evolution of Small Cell Lung
946 Cancer Subtypes by Reprogramming Neuroendocrine Fate. Cancer Cell. 2020. Epub 2020/06/01. doi:
947 10.1016/j.ccell.2020.05.001. PubMed PMID: 32473656.
948 56. Huang YH, Klingbeil O, He XY, Wu XS, Arun G, Lu B, Somerville TDD, Milazzo JP, Wilkinson JE,
949 Demerdash OE, Spector DL, Egeblad M, Shi J, Vakoc CR. POU2F3 is a master regulator of a tuft cell-like
950 variant of small cell lung cancer. Genes Dev. 2018;32(13-14):915-28. Epub 2018/06/28. doi:
951 10.1101/gad.314815.118. PubMed PMID: 29945888; PMCID: PMC6075037.
952 57. Park KS, Liang MC, Raiser DM, Zamponi R, Roach RR, Curtis SJ, Walton Z, Schaffer BE, Roake CM,
953 Zmoos AF, Kriegel C, Wong KK, Sage J, Kim CF. Characterization of the cell of origin for small cell lung
954 cancer. Cell Cycle. 2011;10(16):2806-15. Epub 2011/08/09. doi: 10.4161/cc.10.16.17012. PubMed
955 PMID: 21822053; PMCID: PMC3219544.
956 58. Semenova EA, Nagel R, Berns A. Origins, genetic landscape, and emerging therapies of small cell
957 lung cancer. Genes Dev. 2015;29(14):1447-62. Epub 2015/07/30. doi: 10.1101/gad.263145.115.
958 PubMed PMID: 26220992; PMCID: PMC4526731.
959 59. Yang D, Denny SK, Greenside PG, Chaikovsky AC, Brady JJ, Ouadah Y, Granja JM, Jahchan NS, Lim
960 JS, Kwok S, Kong CS, Berghoff AS, Schmitt A, Reinhardt HC, Park KS, Preusser M, Kundaje A, Greenleaf
961 WJ, Sage J, Winslow MM. Intertumoral Heterogeneity in SCLC Is Influenced by the Cell Type of Origin.
962 Cancer Discov. 2018;8(10):1316-31. Epub 2018/09/20. doi: 10.1158/2159-8290.CD-17-0987.
963 PubMed PMID: 30228179; PMCID: PMC6195211.
964 60. Gazdar AF, Savage TK, Johnson JE, Berns A, Sage J, Linnoila RI, MacPherson D, McFadden DG,
965 Farago A, Jacks T, Travis WD, Brambilla E. The comparative pathology of genetically engineered mouse
966 models for neuroendocrine carcinomas of the lung. J Thorac Oncol. 2015;10(4):553-64. Epub
967 2015/02/13. doi: 10.1097/JTO.0000000000000459. PubMed PMID: 25675280; PMCID: PMC4523224.
968 61. Vivier E, Raulet DH, Moretta A, Caligiuri MA, Zitvogel L, Lanier LL, Yokoyama WM, Ugolini S.
969 Innate or adaptive immunity? The example of natural killer cells. Science. 2011;331(6013):44-9. Epub
970 2011/01/08. doi: 10.1126/science.1198687. PubMed PMID: 21212348; PMCID: PMC3089969.
971 62. Jiang L, Huang J, Higgs BW, Hu Z, Xiao Z, Yao X, Conley S, Zhong H, Liu Z, Brohawn P, Shen D, Wu
972 S, Ge X, Jiang Y, Zhao Y, Lou Y, Morehouse C, Zhu W, Sebastian Y, Czapiga M, Oganesyan V, Fu H, Niu Y,
973 Zhang W, Streicher K, Tice D, Zhao H, Zhu M, Xu L, Herbst R, Su X, Gu Y, Li S, Huang L, Gu J, Han B, Jallal
974 B, Shen H, Yao Y. Genomic Landscape Survey Identifies SRSF1 as a Key Oncodriver in Small Cell Lung
975 Cancer. PLoS Genet. 2016;12(4):e1005895. Epub 2016/04/20. doi: 10.1371/journal.pgen.1005895.
976 PubMed PMID: 27093186; PMCID: PMC4836692.
977 63. Cai L, Lin S, Girard L, Zhou Y, Yang L, Ci B, Zhou Q, Luo D, Yao B, Tang H, Allen J, Huffman K,
978 Gazdar A, Heymach J, Wistuba I, Xiao G, Minna J, Xie Y. LCE: an open web portal to explore gene
979 expression and clinical associations in lung cancer. Oncogene. 2019;38(14):2551-64. Epub
980 2018/12/12. doi: 10.1038/s41388-018-0588-2. PubMed PMID: 30532070; PMCID: PMC6477796.
981 64. Rousseaux S, Debernardi A, Jacquiau B, Vitte AL, Vesin A, Nagy-Mignotte H, Moro-Sibilot D,
982 Brichon PY, Lantuejoul S, Hainaut P, Laffaire J, de Reynies A, Beer DG, Timsit JF, Brambilla C, Brambilla
983 E, Khochbin S. Ectopic activation of germline and placental genes identifies aggressive metastasis-
984 prone lung cancers. Sci Transl Med. 2013;5(186):186ra66. Epub 2013/05/24. doi:
985 10.1126/scitranslmed.3005723. PubMed PMID: 23698379; PMCID: PMC4818008.
986 65. Ruscetti M, Leibold J, Bott MJ, Fennell M, Kulick A, Salgado NR, Chen CC, Ho YJ, Sanchez-Rivera
987 FJ, Feucht J, Baslan T, Tian S, Chen HA, Romesser PB, Poirier JT, Rudin CM, de Stanchina E, Manchado E,
988 Sherr CJ, Lowe SW. NK cell-mediated cytotoxicity contributes to tumor control by a cytostatic drug

989 combination. Science. 2018;362(6421):1416-22. Epub 2018/12/24. doi: 10.1126/science.aas9090.
990 PubMed PMID: 30573629; PMCID: PMC6711172.
991 66. Dang J, Tiwari SK, Lichinchi G, Qin Y, Patil VS, Eroshkin AM, Rana TM. Zika Virus Depletes
992 Neural Progenitors in Human Cerebral Organoids through Activation of the Innate Immune Receptor
993 TLR3. Cell Stem Cell. 2016;19(2):258-65. Epub 2016/05/11. doi: 10.1016/j.stem.2016.04.014.
994 PubMed PMID: 27162029; PMCID: PMC5116380.
995 67. Eden E, Navon R, Steinfeld I, Lipson D, Yakhini Z. GOrilla: a tool for discovery and visualization
996 of enriched GO terms in ranked gene lists. BMC Bioinformatics. 2009;10:48. Epub 2009/02/05. doi:
997 10.1186/1471-2105-10-48. PubMed PMID: 19192299; PMCID: PMC2644678.
998 68. The Gene Ontology C. The Gene Ontology Resource: 20 years and still GOing strong. Nucleic
999 Acids Res. 2019;47(D1):D330-D8. Epub 2018/11/06. doi: 10.1093/nar/gky1055. PubMed PMID:
000 30395331; PMCID: PMC6323945.
001 69. Supek F, Bosnjak M, Skunca N, Smuc T. REVIGO summarizes and visualizes long lists of gene
002 ontology terms. PLoS One. 2011;6(7):e21800. Epub 2011/07/27. doi: 10.1371/journal.pone.0021800.
003 PubMed PMID: 21789182; PMCID: PMC3138752.
004 70. Sergushichev A. An algorithm for fast preranked gene set enrichment analysis using cumulative
005 statistic calculation. bioRxiv. 2016.
006 71. Gu Z, Eils R, Schlesner M. Complex heatmaps reveal patterns and correlations in
007 multidimensional genomic data. Bioinformatics. 2016;32(18):2847-9. Epub 2016/05/22. doi:
008 10.1093/bioinformatics/btw313. PubMed PMID: 27207943.
009 72. Wickham H. ggplot2: Elegant Graphics for Data Analysis. Springer-Verlag New York; 2016.
010 73. Wilke CO. ggridges: Ridgeline Plots in 'ggplot2. 2020.
011 74. Slowikowski K. ggrepel: Automatically Position Non-Overlapping Text Labels with
012 'ggplot2'. 2019.
013 75. Kassambara A. ggpubr: 'ggplot2' Based Publication Ready Plots. 2020.
014 76. Tennekes M. treemap: Treemap Visualization. 2017.
015 77. Neuwirth E. RColorBrewer: ColorBrewer Palettes. 2014.
016 78. Huling J. jcolors: Colors Palettes for R and 'ggplot2', Additional Themes for
017 'ggplot2'. 2020.
018 79. Pedersen TL. patchwork: The Composer of Plots. 2019.
019 80. Davis S, Meltzer PS. GEOquery: a bridge between the Gene Expression Omnibus (GEO) and
020 BioConductor. Bioinformatics. 2007;23(14):1846-7. Epub 2007/05/15. doi:
021 10.1093/bioinformatics/btm254. PubMed PMID: 17496320.
022 81. Bolstad B. preprocessCore: A collection of pre-processing functions. 2019.
023 82. Moon KR, van Dijk D, Wang Z, Gigante S, Burkhardt DB, Chen WS, Yim K, Elzen AVD, Hirn MJ,
024 Coifman RR, Ivanova NB, Wolf G, Krishnaswamy S. Visualizing structure and transitions in high-
025 dimensional biological data. Nat Biotechnol. 2019;37(12):1482-92. Epub 2019/12/05. doi:
026 10.1038/s41587-019-0336-3. PubMed PMID: 31796933; PMCID: PMC7073148.
027 83. Cilloniz C, Pantin-Jackwood MJ, Ni C, Carter VS, Korth MJ, Swayne DE, Tumpey TM, Katze MG.
028 Molecular signatures associated with Mx1-mediated resistance to highly pathogenic influenza virus
029 infection: mechanisms of survival. J Virol. 2012;86(5):2437-46. Epub 2011/12/23. doi:
030 10.1128/JVI.06156-11. PubMed PMID: 22190720; PMCID: PMC3302269.
031 84. Rusinova I, Forster S, Yu S, Kannan A, Masse M, Cumming H, Chapman R, Hertzog PJ.
032 Interferome v2.0: an updated database of annotated interferon-regulated genes. Nucleic Acids Res.
033 2013;41(Database issue):D1040-6. Epub 2012/12/04. doi: 10.1093/nar/gks1215. PubMed PMID:
034 23203888; PMCID: PMC3531205.
035 85. Liberzon A, Birger C, Thorvaldsdottir H, Ghandi M, Mesirov JP, Tamayo P. The Molecular
036 Signatures Database (MSigDB) hallmark gene set collection. Cell Syst. 2015;1(6):417-25. Epub
037 2016/01/16. doi: 10.1016/j.cels.2015.12.004. PubMed PMID: 26771021; PMCID: PMC4707969.

86. Eppig JT. Mouse Genome Informatics (MGI) Resource: Genetic, Genomic, and Biological Knowledgebase for the Laboratory Mouse. ILAR J. 2017;58(1):17-41. Epub 2017/08/26. doi: 10.1093/ilar/ilx013. PubMed PMID: 28838066; PMCID: PMC5886341.
87. Hanzelmann S, Castelo R, Guinney J. GSVA: gene set variation analysis for microarray and RNA-seq data. BMC Bioinformatics. 2013;14:7. Epub 2013/01/18. doi: 10.1186/1471-2105-14-7. PubMed PMID: 23323831; PMCID: PMC3618321.
88. Parra ER, Behrens C, Rodriguez-Canales J, Lin H, Mino B, Blando J, Zhang J, Gibbons DL, Heymach JV, Sepesi B, Swisher SG, Weissferdt A, Kalhor N, Izzo J, Kadara H, Moran C, Lee JJ, Wistuba, II. Image Analysis-based Assessment of PD-L1 and Tumor-Associated Immune Cells Density Supports Distinct Intratumoral Microenvironment Groups in Non-small Cell Lung Carcinoma Patients. Clin Cancer Res. 2016;22(24):6278-89. Epub 2016/06/03. doi: 10.1158/1078-0432.CCR-15-2443. PubMed PMID: 27252415; PMCID: PMC5558040.
89. Fujimoto J, Kadara H, Garcia MM, Kabbout M, Behrens C, Liu DD, Lee JJ, Solis LM, Kim ES, Kalhor N, Moran C, Sharafkhaneh A, Lotan R, Wistuba, II. G-protein coupled receptor family C, group 5, member A (GPRC5A) expression is decreased in the adjacent field and normal bronchial epithelia of patients with chronic obstructive pulmonary disease and non-small-cell lung cancer. J Thorac Oncol. 2012;7(12):1747-54. Epub 2012/11/17. doi: 10.1097/JTO.0b013e31826bb1ff. PubMed PMID: 23154545; PMCID: PMC3622592.
90. Tang C, Hobbs B, Amer A, Li X, Behrens C, Canales JR, Cuentas EP, Villalobos P, Fried D, Chang JY, Hong DS, Welsh JW, Sepesi B, Court L, Wistuba, II, Koay EJ. Development of an Immune-Pathology Informed Radiomics Model for Non-Small Cell Lung Cancer. Sci Rep. 2018;8(1):1922. Epub 2018/02/02. doi: 10.1038/s41598-018-20471-5. PubMed PMID: 29386574; PMCID: PMC5792427.
91. Gautier L, Cope L, Bolstad BM, Irizarry RA. affy--analysis of Affymetrix GeneChip data at the probe level. Bioinformatics. 2004;20(3):307-15. Epub 2004/02/13. doi: 10.1093/bioinformatics/btg405. PubMed PMID: 14960456.
92. Dai M, Wang P, Boyd AD, Kostov G, Athey B, Jones EG, Bunney WE, Myers RM, Speed TP, Akil H, Watson SJ, Meng F. Evolving gene/transcript definitions significantly alter the interpretation of GeneChip data. Nucleic Acids Res. 2005;33(20):e175. Epub 2005/11/15. doi: 10.1093/nar/gni179. PubMed PMID: 16284200; PMCID: PMC1283542.
93. Dobin A, Davis CA, Schlesinger F, Drenkow J, Zaleski C, Jha S, Batut P, Chaisson M, Gingeras TR. STAR: ultrafast universal RNA-seq aligner. Bioinformatics. 2013;29(1):15-21. Epub 2012/10/30. doi: 10.1093/bioinformatics/bts635. PubMed PMID: 23104886; PMCID: PMC3530905.
94. Trapnell C, Williams BA, Pertea G, Mortazavi A, Kwan G, van Baren MJ, Salzberg SL, Wold BJ, Pachter L. Transcript assembly and quantification by RNA-Seq reveals unannotated transcripts and isoform switching during cell differentiation. Nat Biotechnol. 2010;28(5):511-5. Epub 2010/05/04. doi: 10.1038/nbt.1621. PubMed PMID: 20436464; PMCID: PMC3146043.
95. Bullard JH, Purdom E, Hansen KD, Dudoit S. Evaluation of statistical methods for normalization and differential expression in mRNA-Seq experiments. BMC Bioinformatics. 2010;11:94. Epub 2010/02/20. doi: 10.1186/1471-2105-11-94. PubMed PMID: 20167110; PMCID: PMC2838869.
96. Ritz C, Baty F, Streibig JC, Gerhard D. Dose-Response Analysis Using R. PLoS One. 2015;10(12):e0146021. Epub 2015/12/31. doi: 10.1371/journal.pone.0146021. PubMed PMID: 26717316; PMCID: PMC4696819.
97. McMillan EA, Ryu MJ, Diep CH, Mendiratta S, Clemenceau JR, Vaden RM, Kim JH, Motoyaji T, Covington KR, Peyton M, Huffman K, Wu X, Girard L, Sung Y, Chen PH, Mallipeddi PL, Lee JY, Hanson J, Voruganti S, Yu Y, Park S, Sudderth J, DeSevo C, Muzny DM, Doddapaneni H, Gazdar A, Gibbs RA, Hwang TH, Heymach JV, Wistuba I, Coombes KR, Williams NS, Wheeler DA, MacMillan JB, Deberardinis RJ, Roth MG, Posner BA, Minna JD, Kim HS, White MA. Chemistry-First Approach for Nomination of Personalized Treatment in Lung Cancer. Cell. 2018;173(4):864-78 e29. Epub 2018/04/24. doi: 10.1016/j.cell.2018.03.028. PubMed PMID: 29681454; PMCID: PMC5935540.

Figures

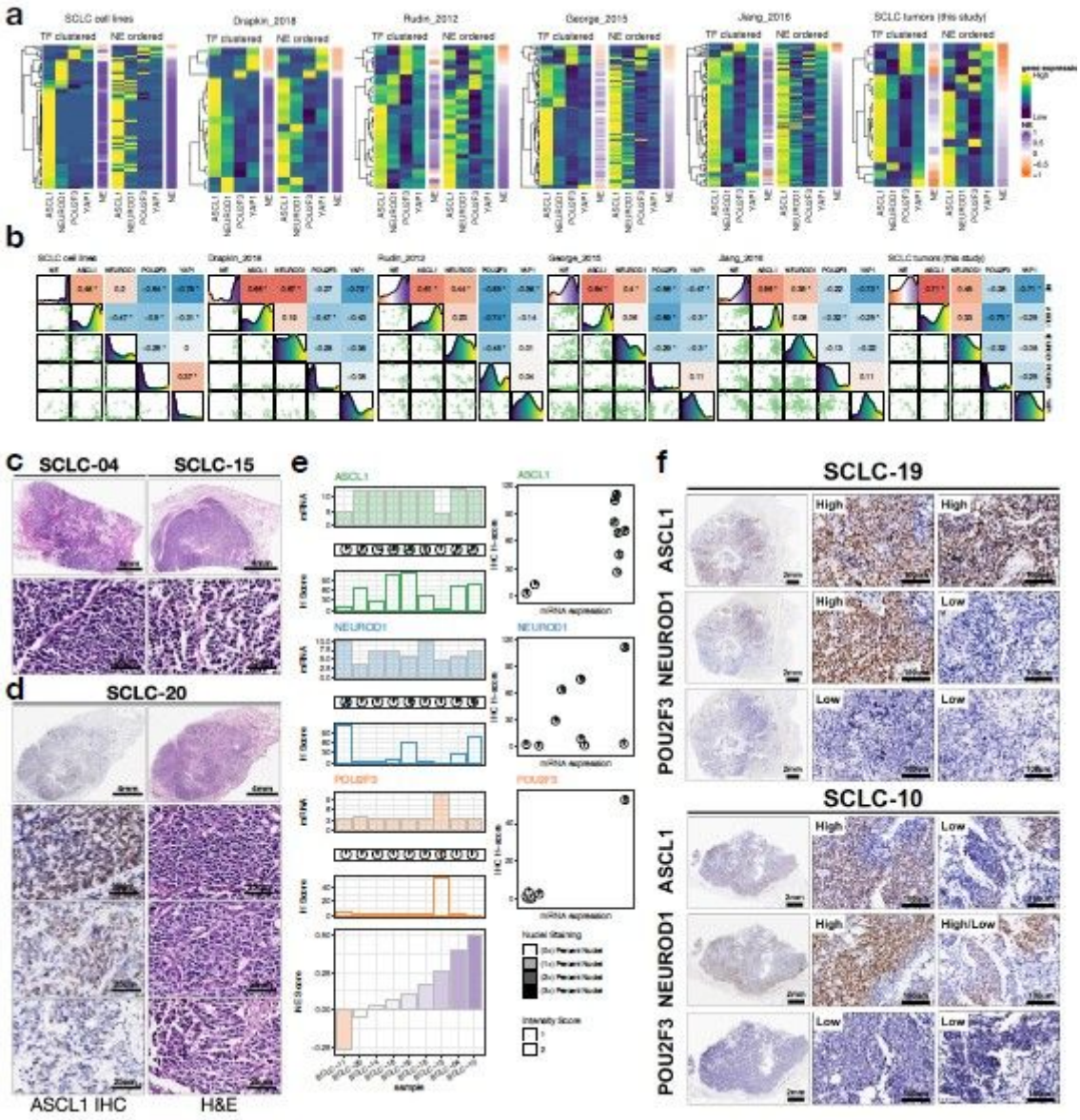

Figure 1

NE score and SCLC molecular subtypes a, Heatmaps visualizing expression of molecular subtype-specific TFs and NE scores. Two heatmaps were generated for each study, with one ordered by complete linkage hierarchical clustering of TFs and the other ordered by NE scores. b, Pairwise associations among NE scores and molecular subtype-specific TFs. Lower left panels are scatter plots, diagonal line panels are density plots and upper right panel shows correlation coefficients from pairwise Pearson correlation. *, p-value < 0.05. c, H&E staining of two high NE score SCLC tumor samples showing classic SCLC morphology with dark nuclei, scant cytoplasm and inconspicuous nucleoli. d, ASCL1 IHC staining and H&E staining of a low NE-score SCLC tumor, showing variable morphology at different selected areas, where ASCL1-low areas appear to be more variant-like e, Quantifications of TF expression from IHC staining or microarray profiling, samples are ordered by increasing NE scores. f, IHC of ASCL1, NEUROD1

and POU2F3 in two tumors that express both ASCL1and NEUROD1. Two areas per tumor were selected for showing intratumoral heterogeneity in ASCL1 and NEUROD1 expression patterns.

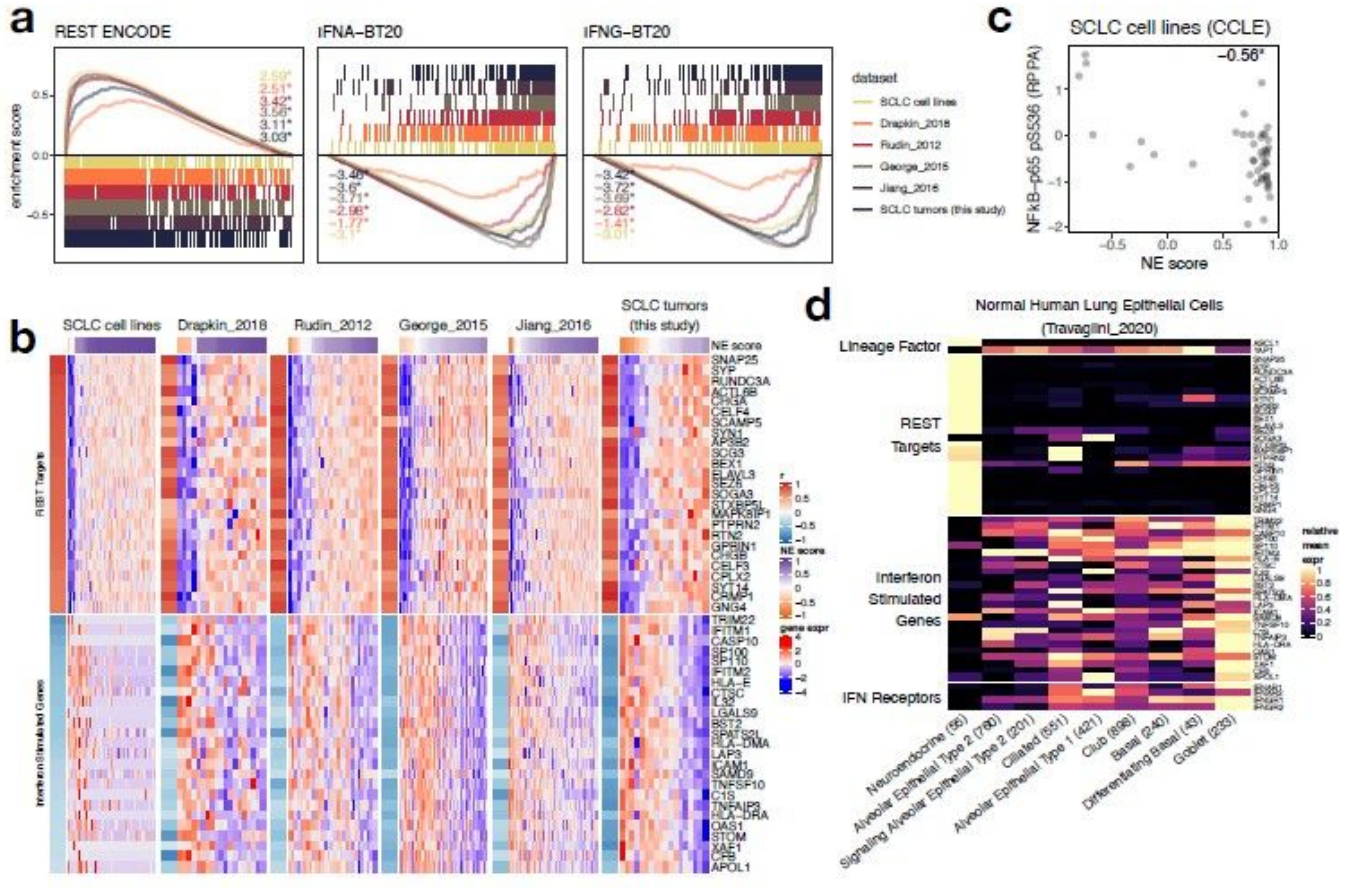

Figure 2

Repression of ISGs in high NE-score SCLC and PNECs a, GSEA enrichment plots for selected genesets. Results from SCLC cell lines, PDXs (Drapkin_2018) and patient tumor datasets were superimposed. Normalized enrichment score (NES) were provided. *, multiple comparison adjusted p-value < 0.05. b, Heatmaps for top 25 leading edge genes selected from genesets in (a). Gene expression matrix of each dataset was annotated with color-coded Pearson correlation coefficient (from correlating NE score with gene expression) as a left-side column, and a top bar indicating NE scores. c, Scatter plots showing negative correlation between NE score and Ser536 phosphorylation on NFkB-p65 in SCLC cell lines. Pearson correlation coefficient was provided. *, p-value < 0.05. d, Heatmap showing relative expression of selected lineage factors (ASCL1 and YAP1), REST targets and ISGs (same genes as used in b, determined from a) as well as interferon receptor genes in healthy human lung epithelial cells based on scRNA-seq experiments.

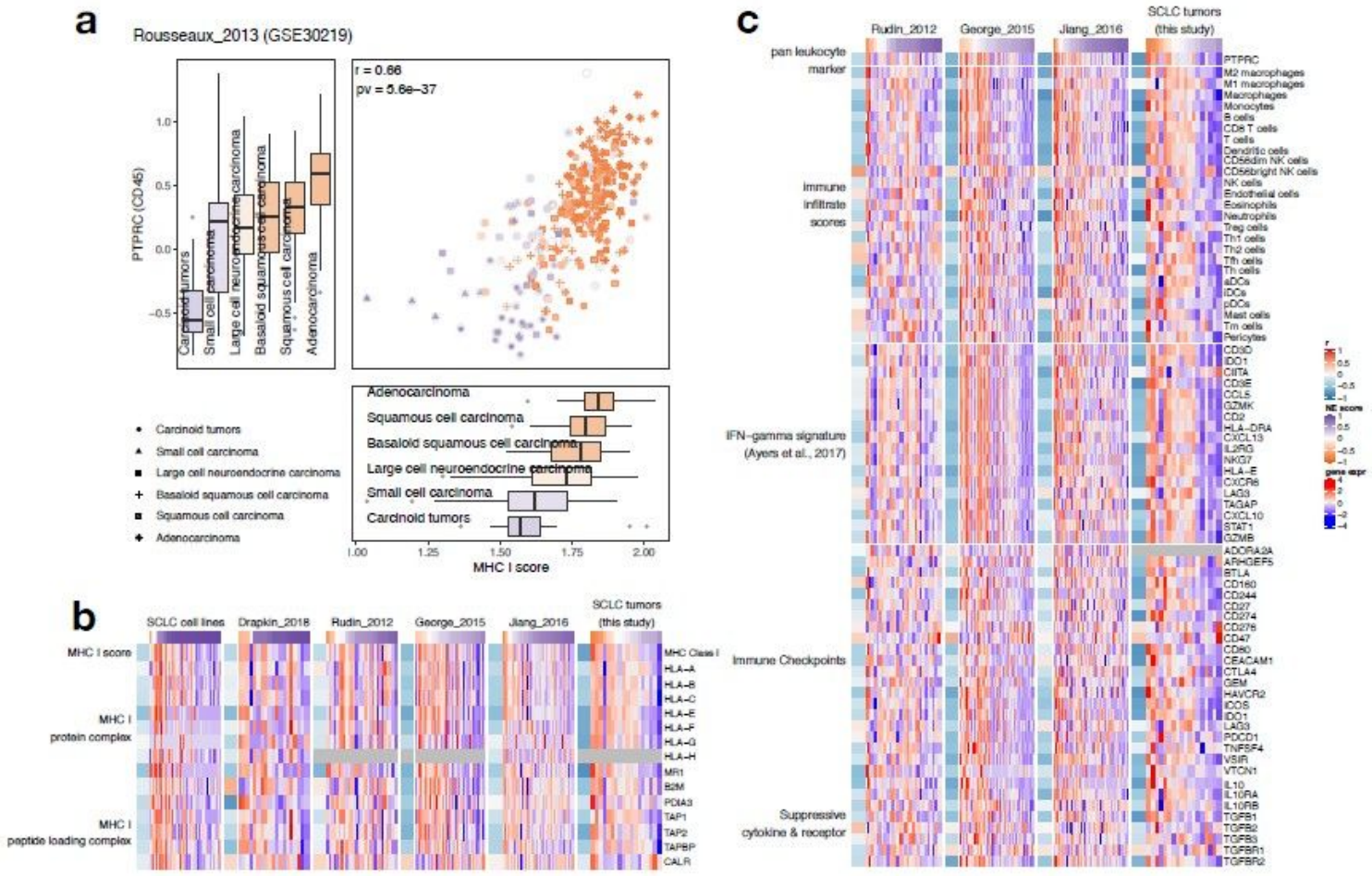

Figure 3

Low NE-score variant SCLC have increased tumor-immune interaction a, Expression of MHC I genes and pan-leukocyte marker PTPRC 361 in lung tumors from the “Rousseaux_2013” dataset. Box whisker plots are filled with color reflecting the median NE score in different histological subtypes. Color for scatterplot symbols reflects NE score for different samples. b, Heatmaps visualizing expression of MHC I genes across multiple SCLC datasets. c, Heatmaps visualizing expression of PTPRC, immune-cell-type-specific signature scores, PD-1 blockade response-predicting IFN gamma related signature genes (46), immune checkpoint genes and suppressive cytokines and receptors in SCLC tumor datasets.

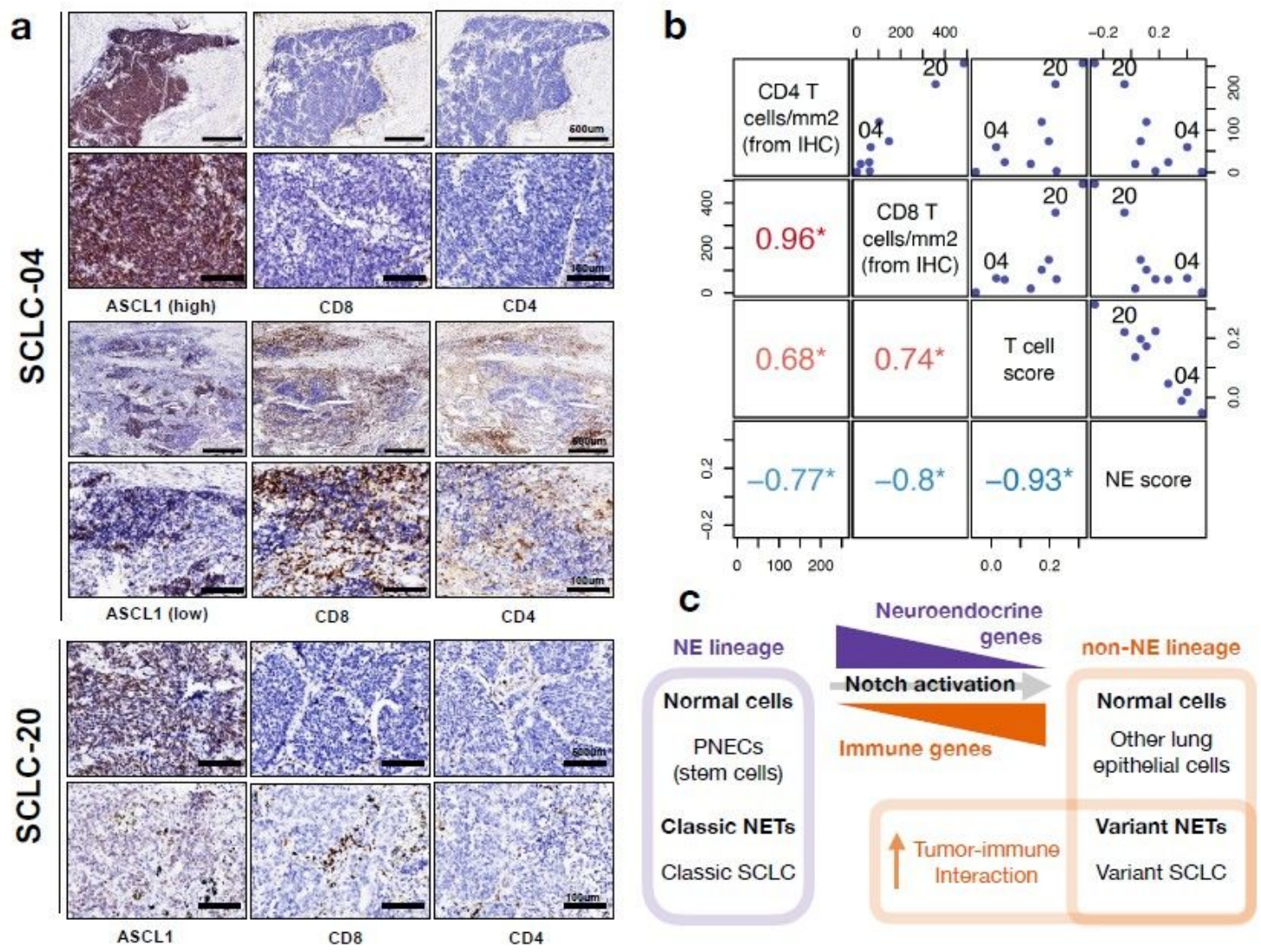

Figure 4

Intertumoral and intratumoral heterogeneity in T cell infiltration from SCLC tumors with variable NE features a, IHC of ASCL1, CD4 and CD8 in selected tumors. SCLC-04 is a SCLC tumor with NE score of 0.4. CD8 or CD4 T cells were few in the ASCL1-high regions but abundant in the ASCL1-low region; SCLC-20 is a tumor with NE score of -0.05, similar reciprocal relationship of ASCL1 staining and T cell infiltration was observed. Representative regions with high or low ASCL1 staining were shown. b, Relationship between IHC-determined per area CD4 and CD8 T cell count, gene expression-based T cell score and NE score in all 9 tumors assessed. Scatter plots and Pearson correlation coefficients were provided for assessment of pairwise correlations. *, Pearson correlation with p-value < 0.05. c, Schematic diagram showing relationship between neuroendocrine and immune gene expression in normal cells and neuroendocrine tumors (NETs).

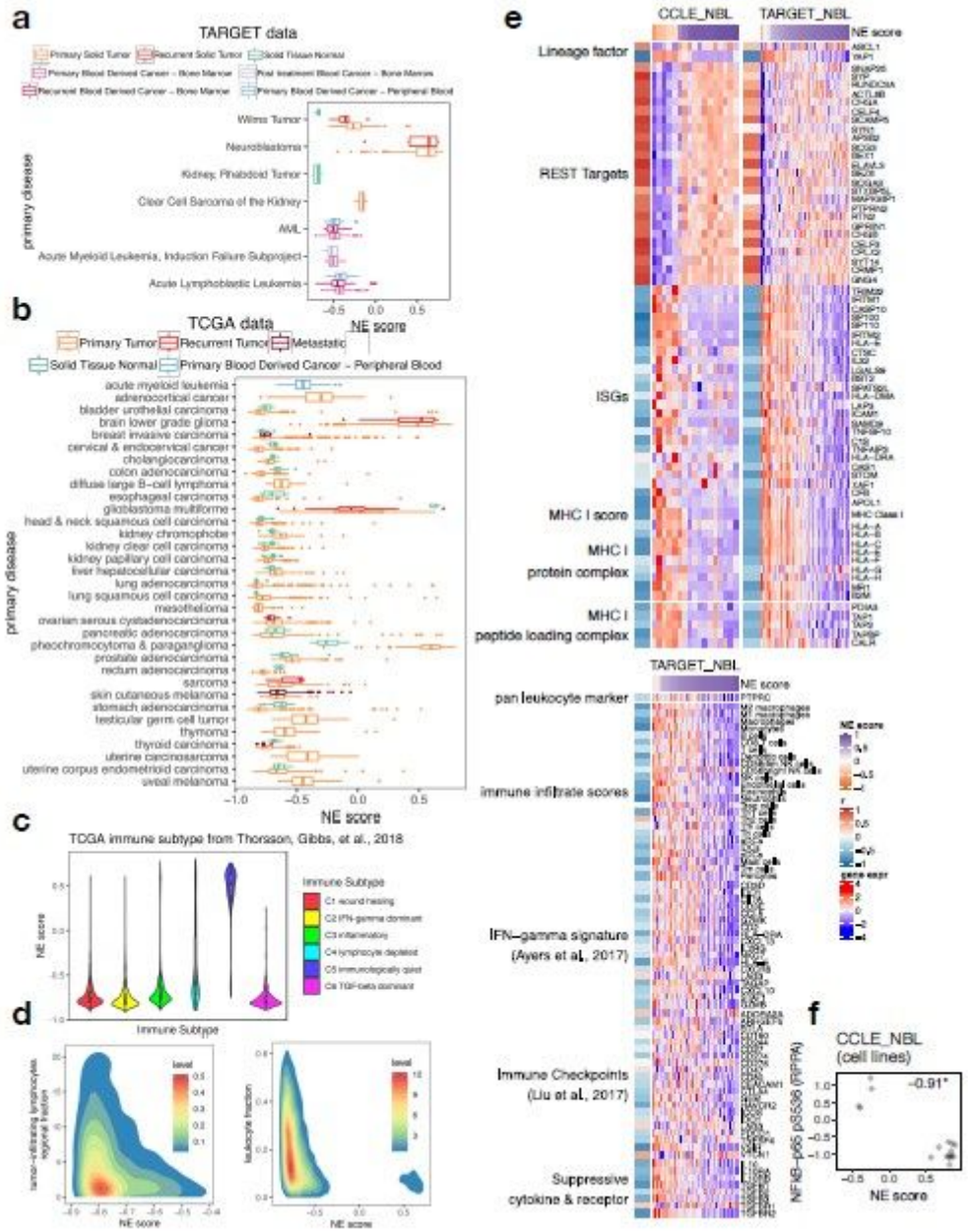

Figure 5

Relationship between NE scores and immune phenotypes in pan-cancer samples a-b, NE scores of pan-cancer samples in the TARGET pediatric cancer cohorts (a) and TCGA adult cancer cohorts (b). c, NE scores by immune subtype in TCGA pan-cancer samples. d, Relationship between NE scores and tumor-infiltrating lymphocytes regional fraction or leukocyte fraction in TCGA pan-cancer samples. e, Heatmap visualizing expression of various genes and summary scores previously assessed for SCLC and now in NBL with cell line and tumor datasets side-by-side. f, Scatter plots showing negativecorrelation between NE score and Ser536 phosphorylation on NFkB-p65 in NBL cell lines. Pearson correlation coefficient was provided. *, p-value < 0.05.

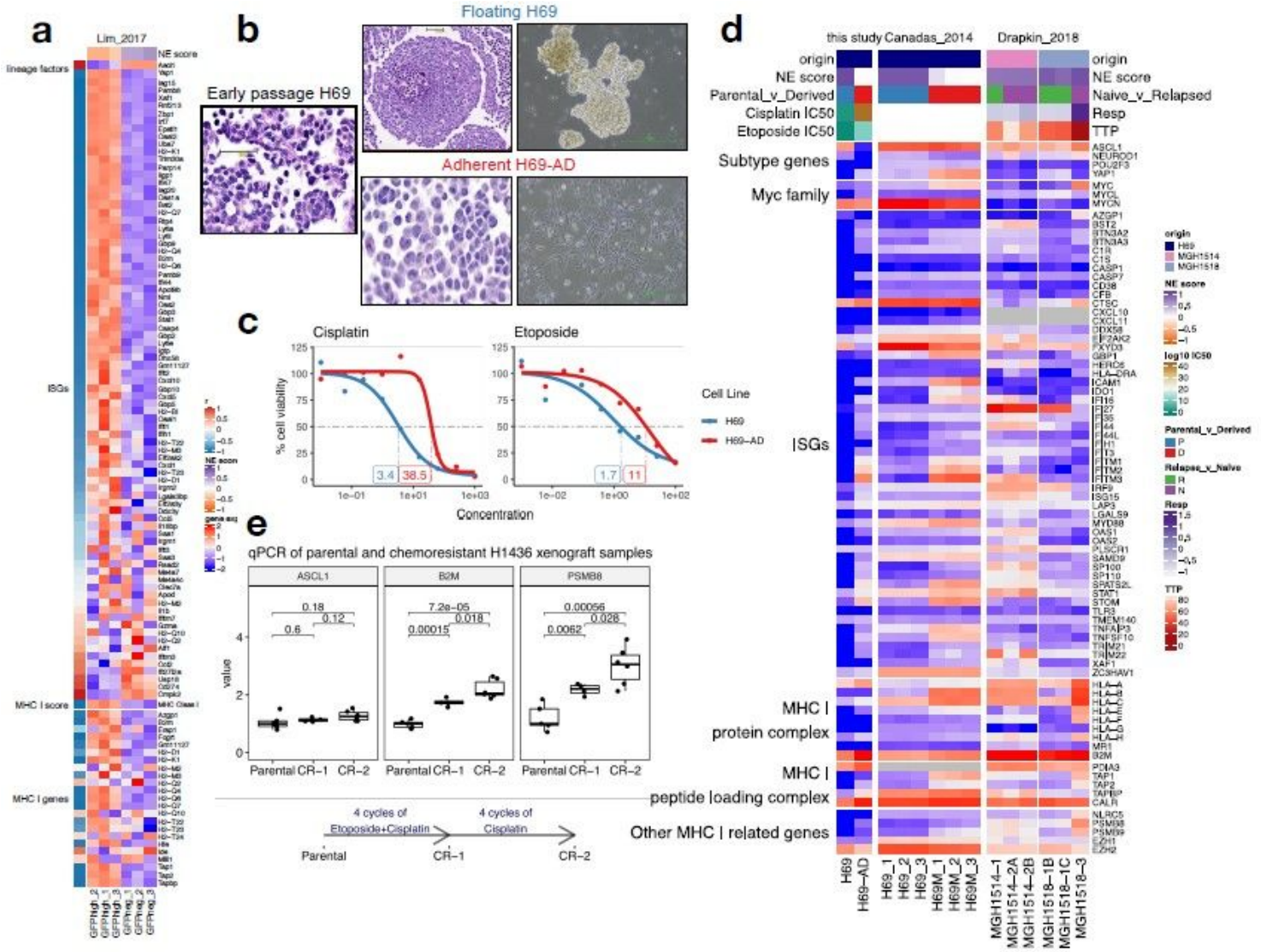

Figure 6

MHC I upregulation in chemoresistant 389 SCLC a, Heatmap visualizing increased expression of ISGs, MHC I genes as cells switch from Ascl1+ to Yap1+ in SCLC GEMM tumors from the “Lim_2017” . GFP was expressed from endogenous promoter of a Notch target gene Hes1 in Rb-/-/p53-/-/p130-/- (TKO) background. Using flow cytometry, the authors first sorted out SCLC tumor cells and then further sorted by GFP to obtain relatively pure tumor cells with different Notch activation status. Three biological replicates were each provided for GFP negative (Notch inactive, classic high-NE) cells and GFP positive cells (Notch active, low-NE). b, Different morphology and culture characteristics of adherent H69-AD and the parental H69. c, Dose response curves for Cisplatin and Etoposide in the H69 cell line pair. Note that H69-AD, the adherent line, is more resistant with higher IC50s. d, Expression changes of selected genes in: H69 cell line pair from this study, H69 and derived mesenchymal H69M cell lines from “Canadas_2014” and autologous PDX samples before and after chemotherapy from “Drapkin_2018”. PDX parameters: TTP, time to progression, defined by time to 2x initial tumor volume; RESP, change in tumor volume between initial tumor volume and minimum of day 14-28. Relapsed sample from MGH-1514 did not show increased chemoresistance based on the RESP and TTP parameters. Note that unlike other heatmaps,

due to the small number of samples in each dataset, expression is not scaled by gene in this heatmap. e, qPCR measurement of normalized ASCL1, B2M and PSMB8 expression in naïve parental and chemoresistant H1436 xenograft tumors.

Supplementary Files

This is a list of supplementary files associated with this preprint. Click to download.

- supplementaryfigures.pdf
- nrreportingsummary.pdf
- supplementarytables.xlsx